ALERT Geomaterials

Mechanical characterization of porous sandstones in true triaxial conditions: diffuse and localized deformation, effect of anisotropy

presentation by

Cyrille Couture

for the Ioannis Vardoulakis PhD Prize

September 28th 2021

32nd ALERT workshop and school in Aussois

Introduction

My PhD thesis has been focused on:

- true triaxial loading paths ($\sigma_1 > \sigma_2 > \sigma_3$) naturaly occuring in subsurface reservoirs of sedimentary rocks (isotropic and anisotropic porous sandstones)

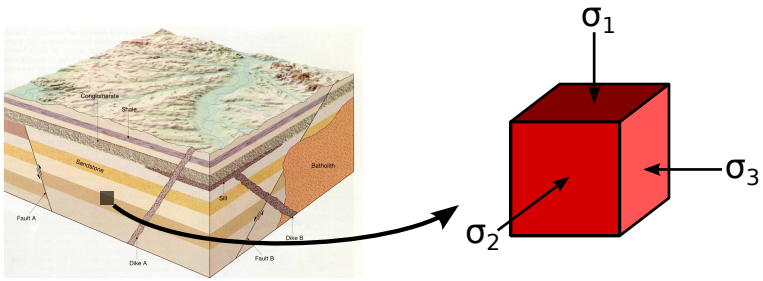

Introduction

My PhD thesis has been focused on:

- true triaxial loading paths ($\sigma_1 > \sigma_2 > \sigma_3$) naturaly occuring in subsurface reservoirs of sedimentary rocks (isotropic and anisotropic porous sandstones)

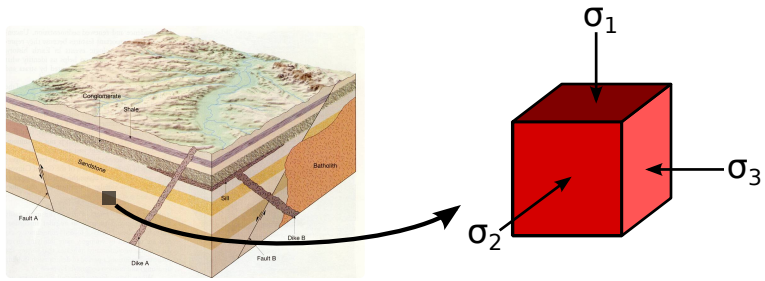

- the multiscale aspects of heterogeneities (random and organized distributions) and localized deformation

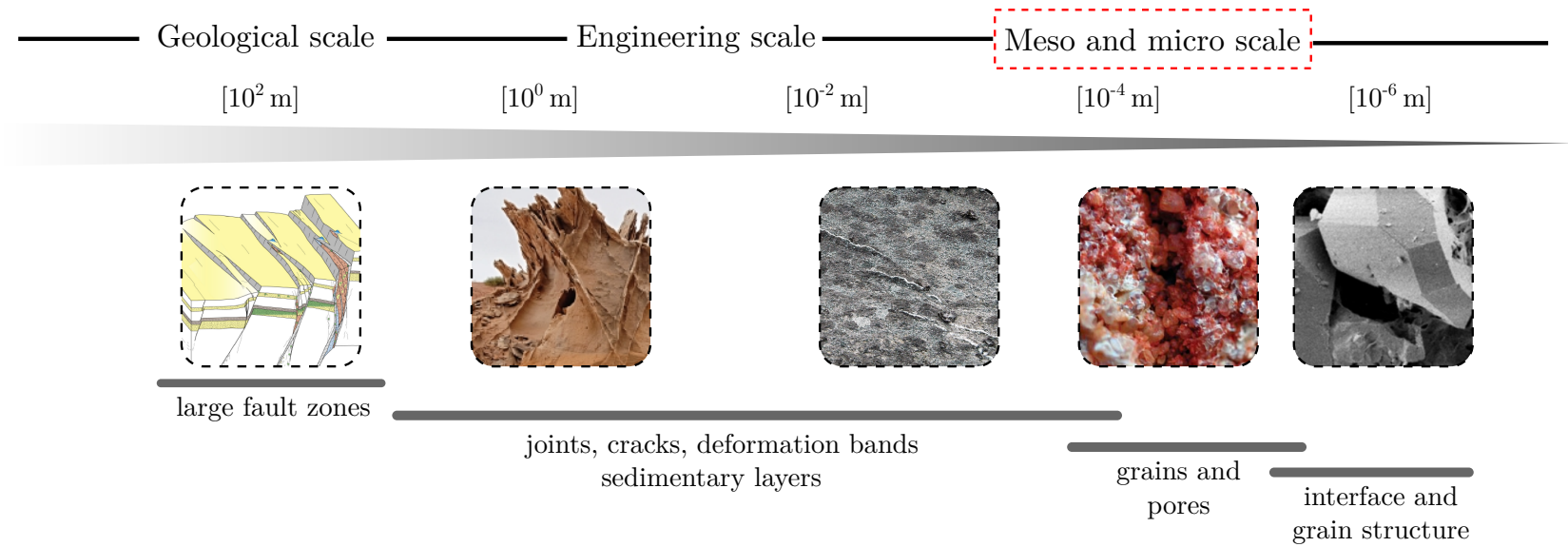

Scope of the presentation

Experimental study

- The role of the Lode angle on the mecanical response and localized deformation (true triaxial loading)

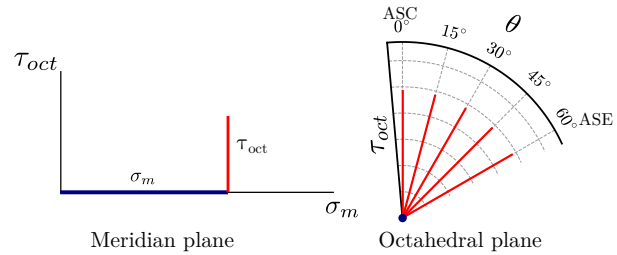

Scope of the presentation

Experimental study

- The role of the Lode angle on the mecanical response and localized deformation (true triaxial loading)

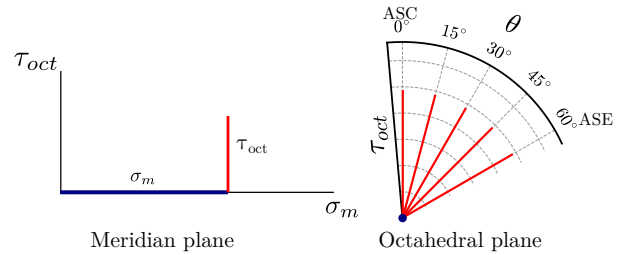

- Combined with bedding plane anisotropy

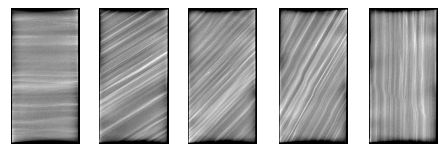

Scope of the presentation

Experimental study

- The role of the Lode angle on the mecanical response and localized deformation (true triaxial loading)

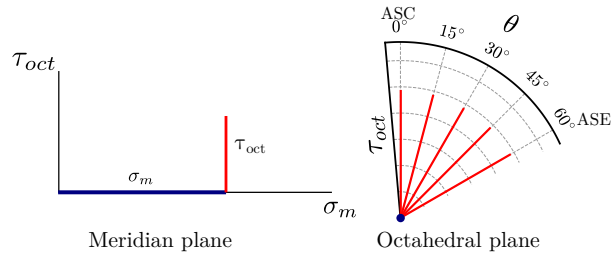

- Combined with bedding plane anisotropy

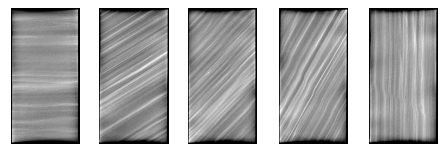

Theoretical study

- Prediction of deformation bands kinematic using a bifurcation model

Scope of the presentation

Experimental study

- The role of the Lode angle on the mecanical response and localized deformation (true triaxial loading)

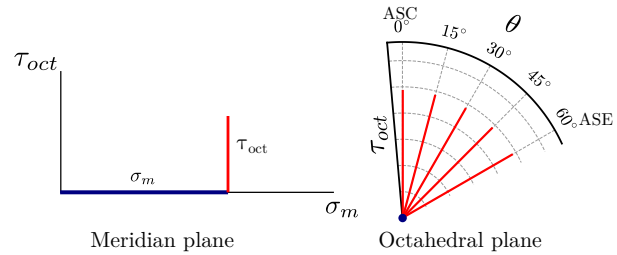

- Combined with bedding plane anisotropy

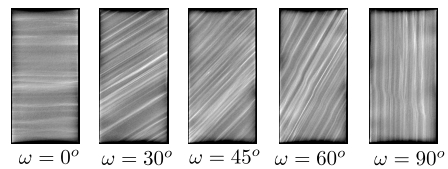

Theoretical study

- Prediction of deformation bands kinematic using a bifurcation model

Numerical study

- Multiscale simulations with a coupled FEMxDEM model

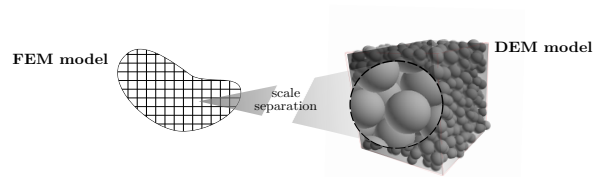

Scope of the presentation

Experimental study

- The role of the Lode angle on the mecanical response and localized deformation (true triaxial loading)

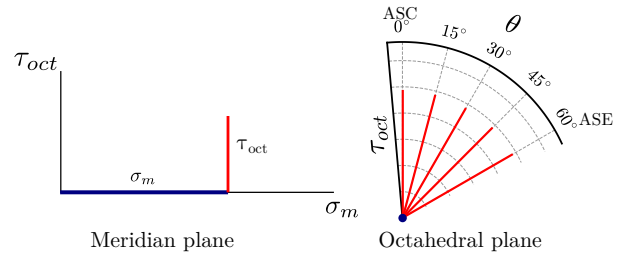

- Combined with bedding plane anisotropy

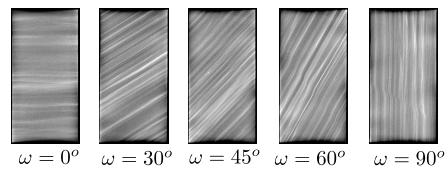

Theoretical study

- Prediction of deformation bands kinematic using a bifurcation model

Numerical study

- Multiscale simulations with a coupled FEMxDEM model

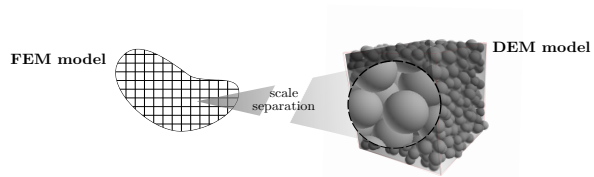

- Comparison of results with experimental observations

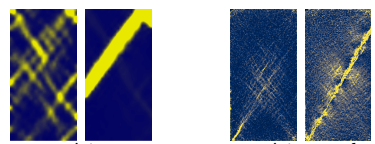

True triaxial experiments: experimental setup

True triaxial apparatus at Laboratoire 3SR

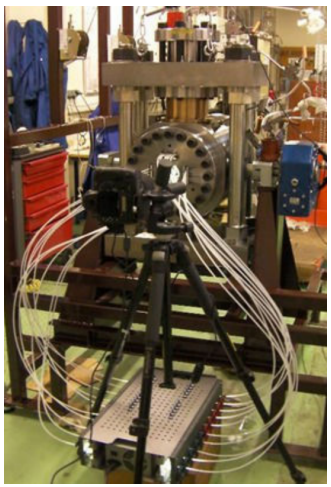

Experimental setup

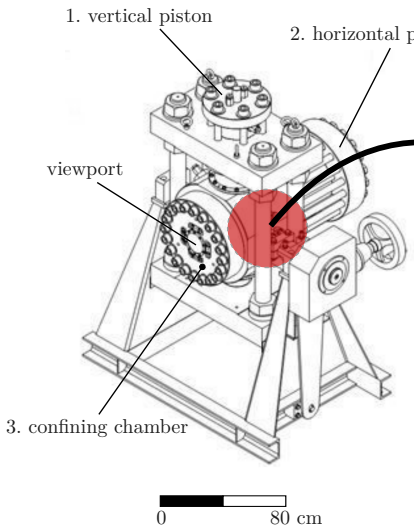

Schematic of the apparatus

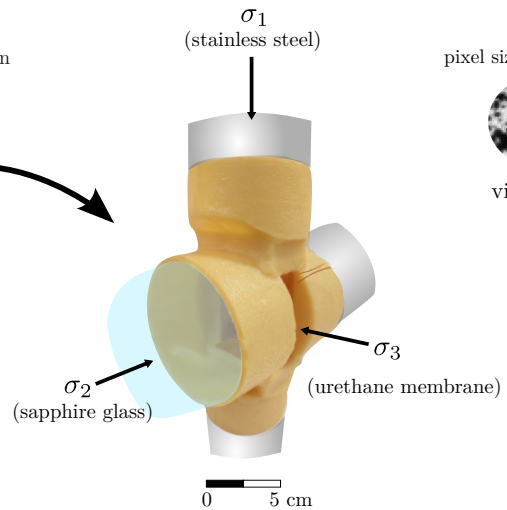

Isolating membrane inside the confining chamber

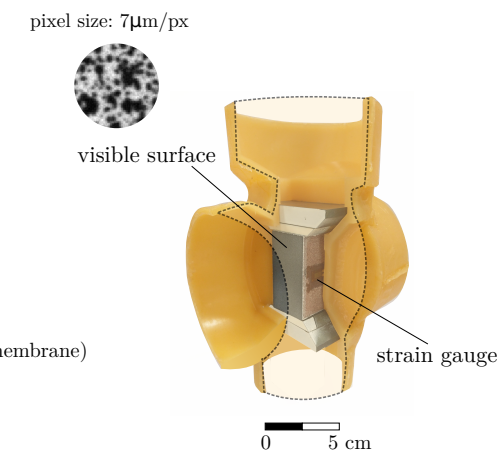

See through view of the sample

Experimental developments:

- Protocol for corrected and stress invariants controled loading paths
- Enhancement of critical loading components (friction reduction, membrane preparation) and acquisition methods (speckle patterns, strain gauge for out of plane deformation measurement)

Acquisition and correlation of optical images during the loading phase

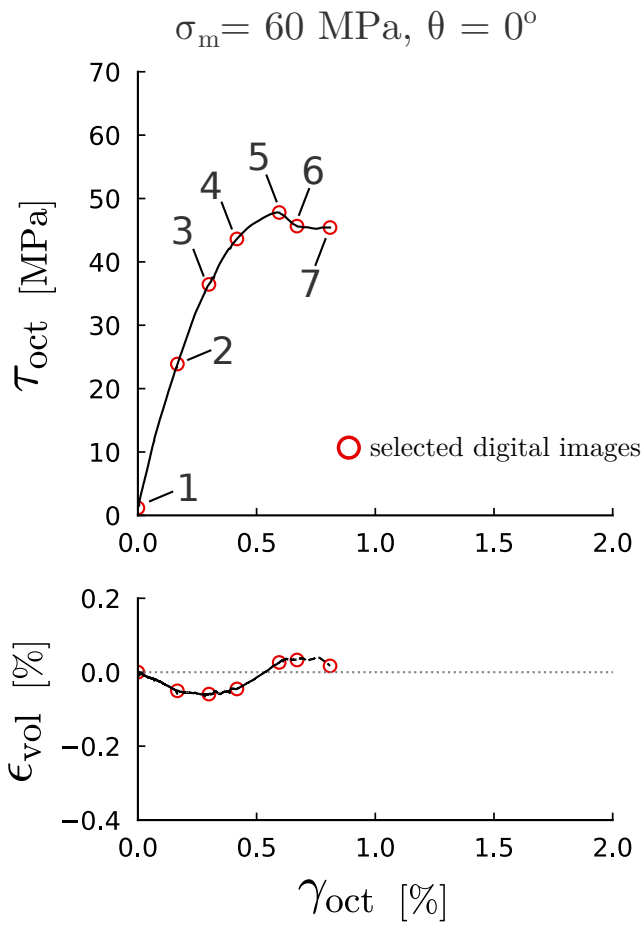

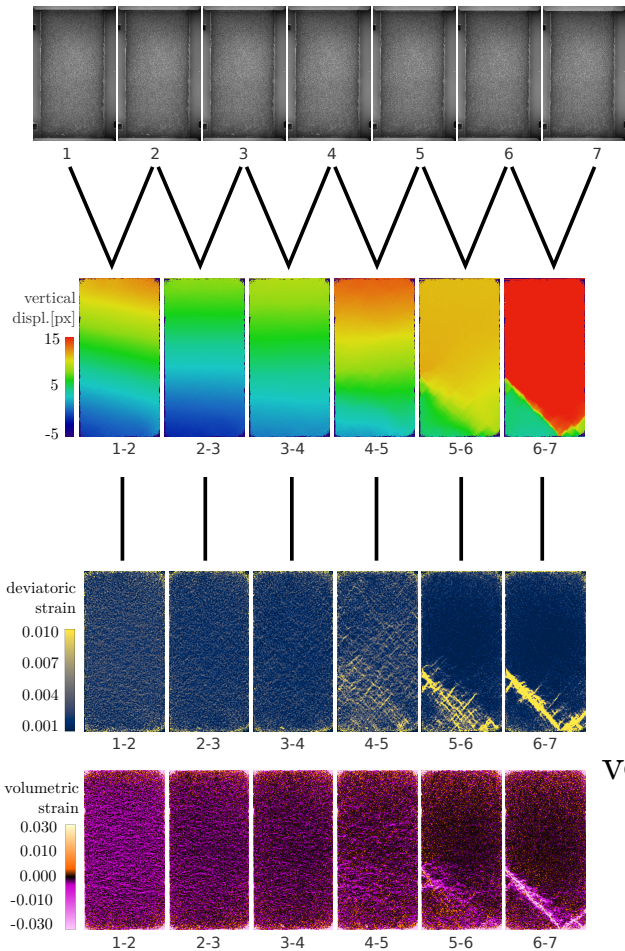

image sequence

incremental displacement field (local DIC)

deviatoric and volumetric deformations

DIC performed using spam [Stamati et al., 2020]

Isotropic Vosges sandstone (21% porosity)

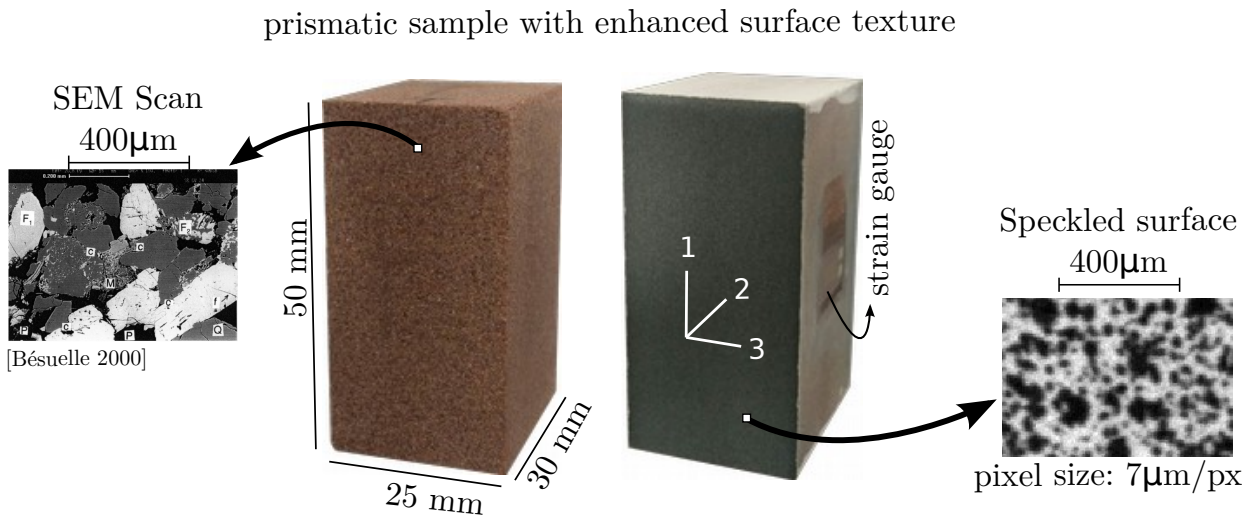

Isotropic Vosges sandstone (21% porosity)

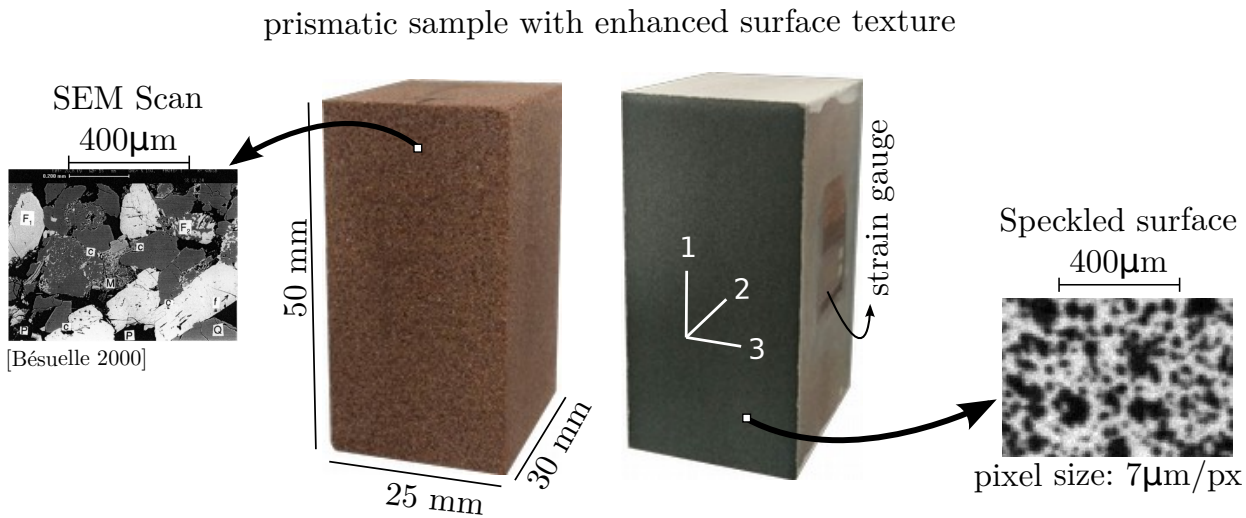

Experimental campaign on 10 samples

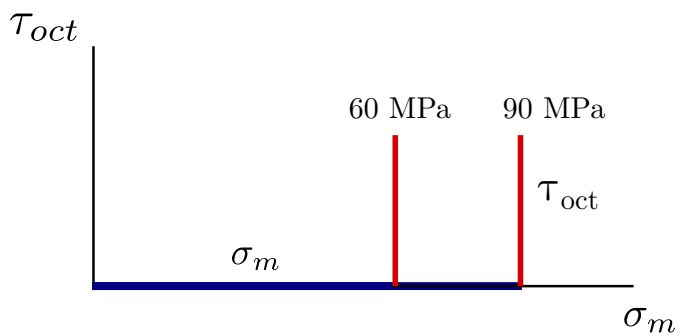

meridian plane (constant θ)

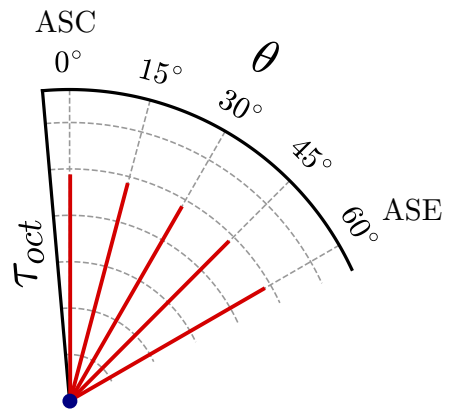

octahedral plane (constant σ_m)

True triaxial experiments: isotropic sandstone

Octahedral stress-strain curves

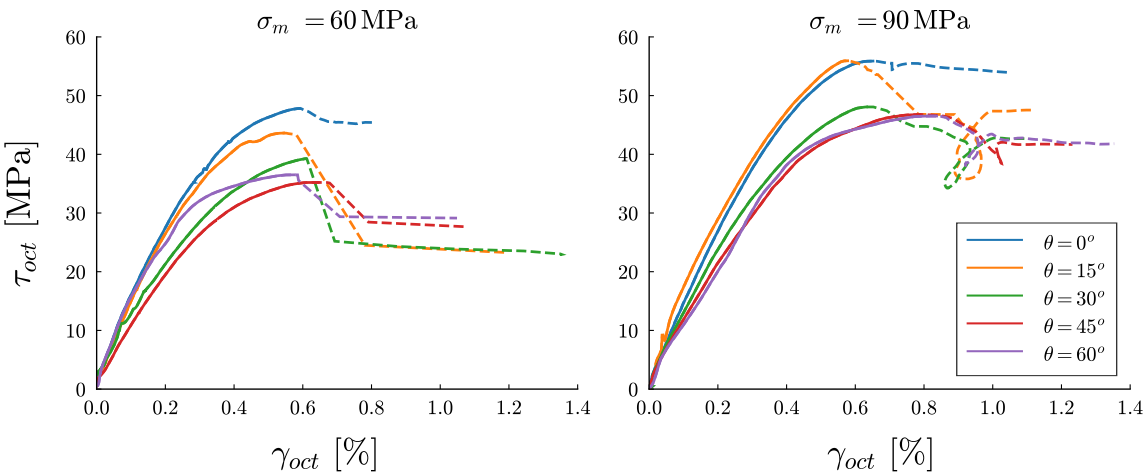

Octahedral stress peak

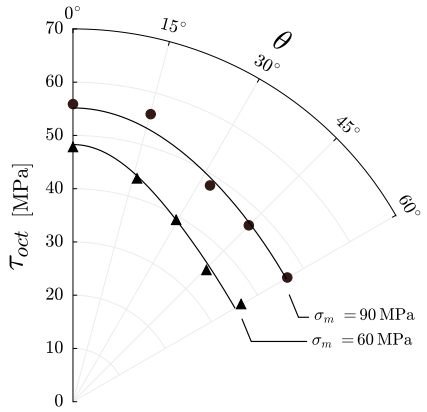

True triaxial experiments: isotropic sandstone

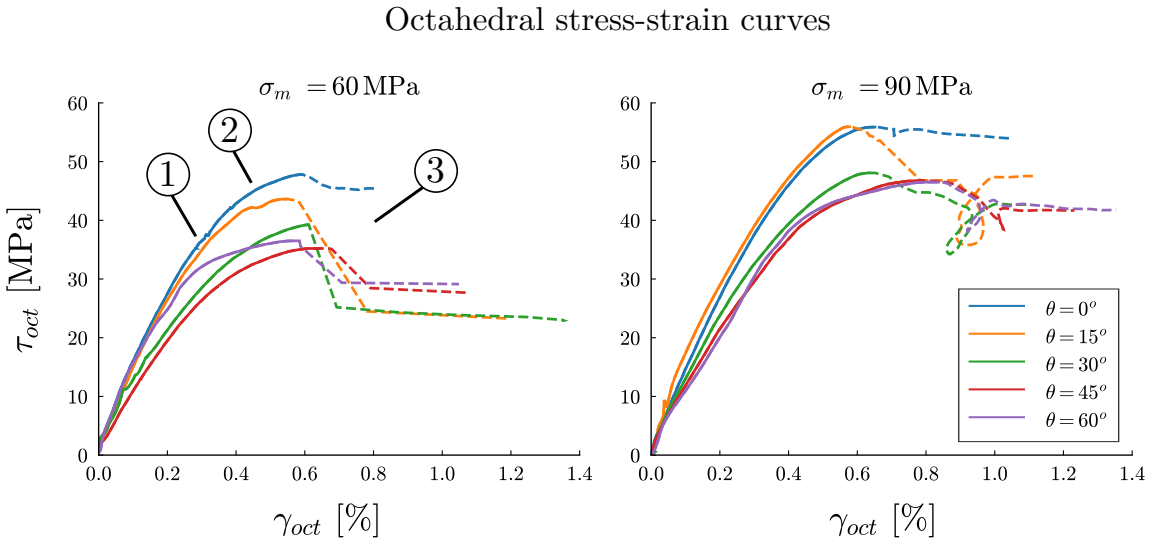

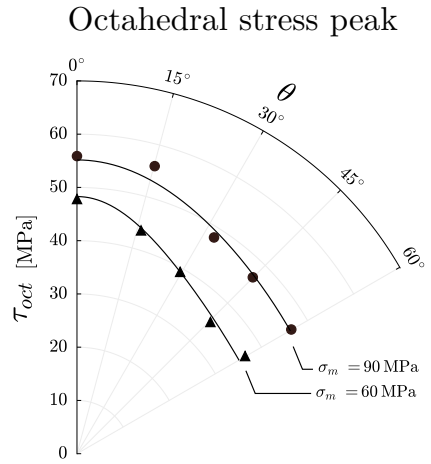

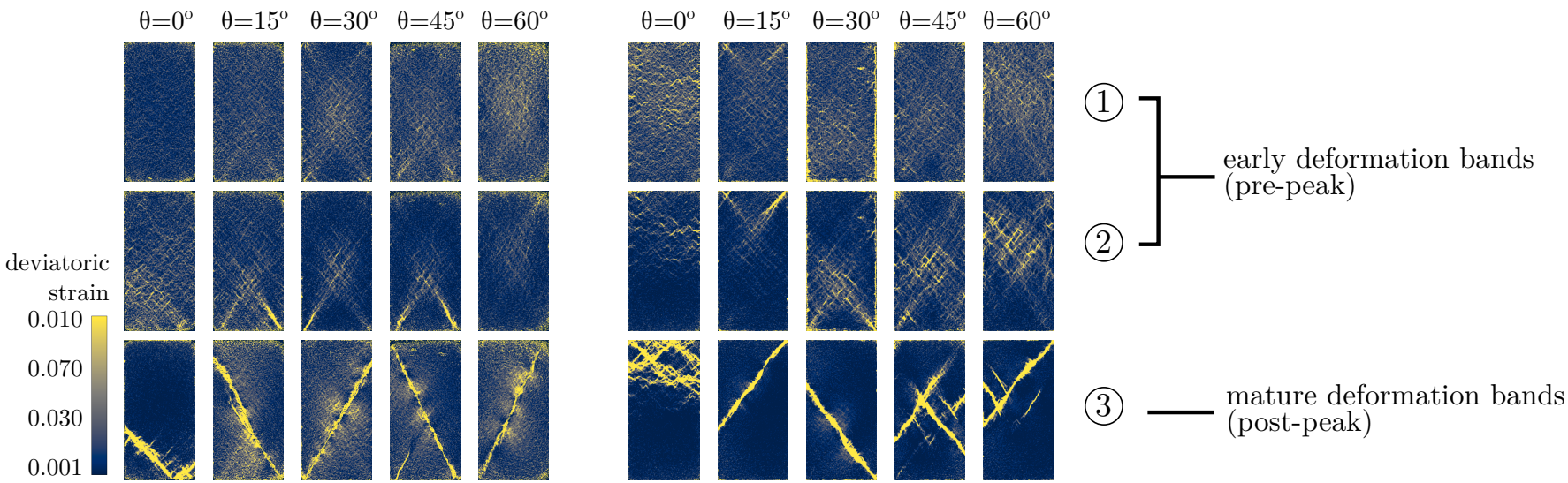

True triaxial experiments: isotropic sandstone

Octahedral stress-strain curves

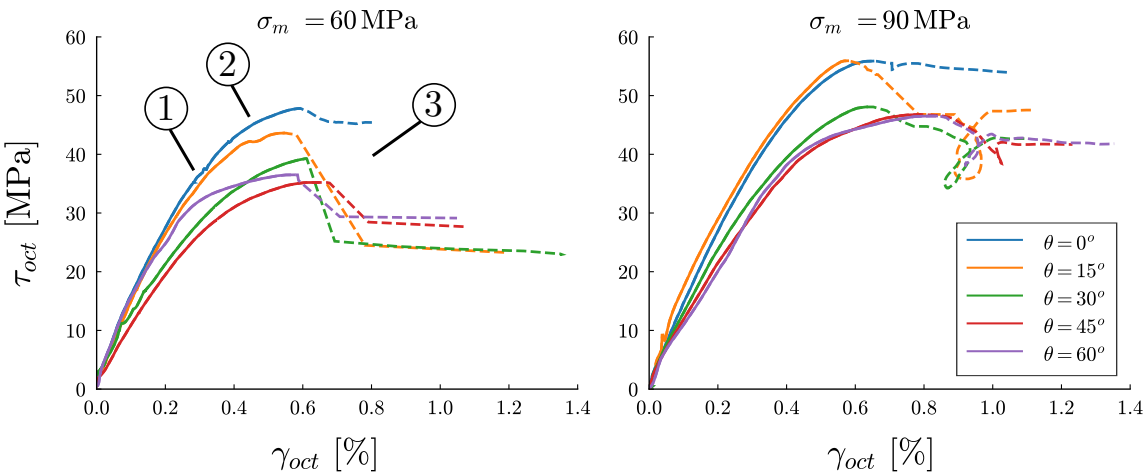

Octahedral stress peak

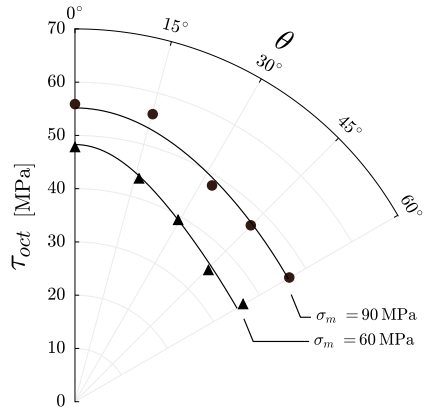

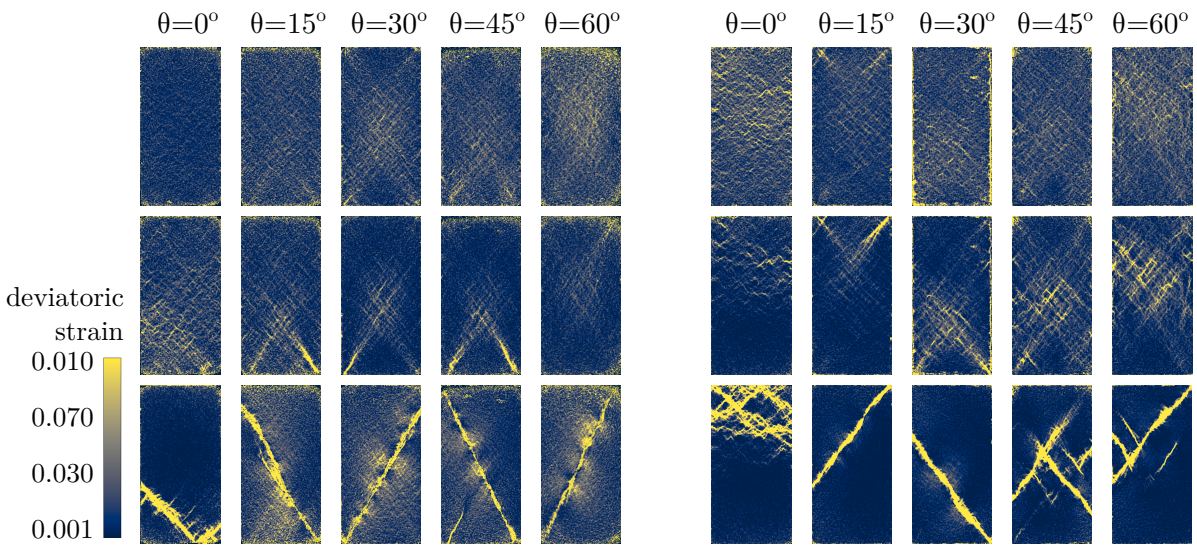

deformation band angle

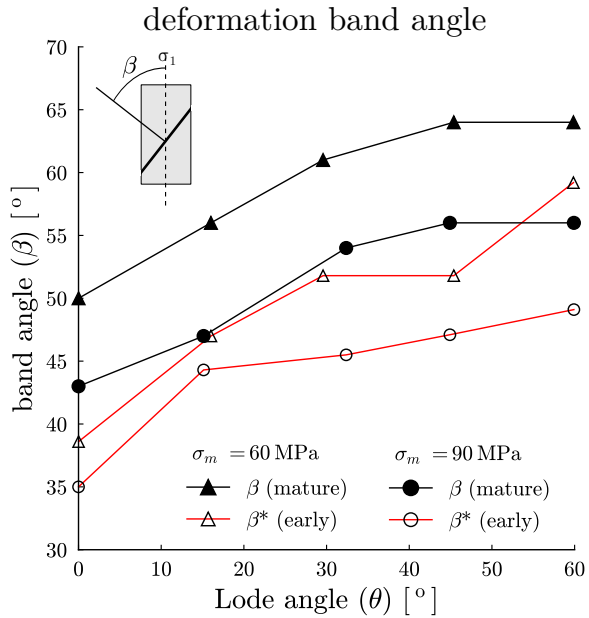

Evolution of localized deformation by full-field measurements during the loading phase

- Brittle behavior: at low mean stress and high Lode angle

  σ_m= 60 MPa, $\theta = 45^o$

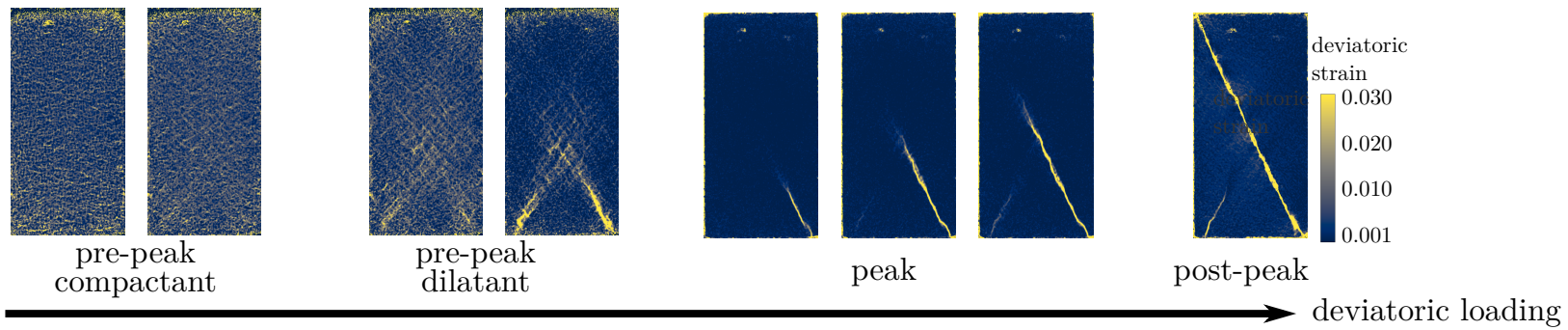

Evolution of localized deformation by full-field measurements during the loading phase

- Brittle behavior: at low mean stress and high Lode angle

  σ_m= 60 MPa, $\theta = 45^o$

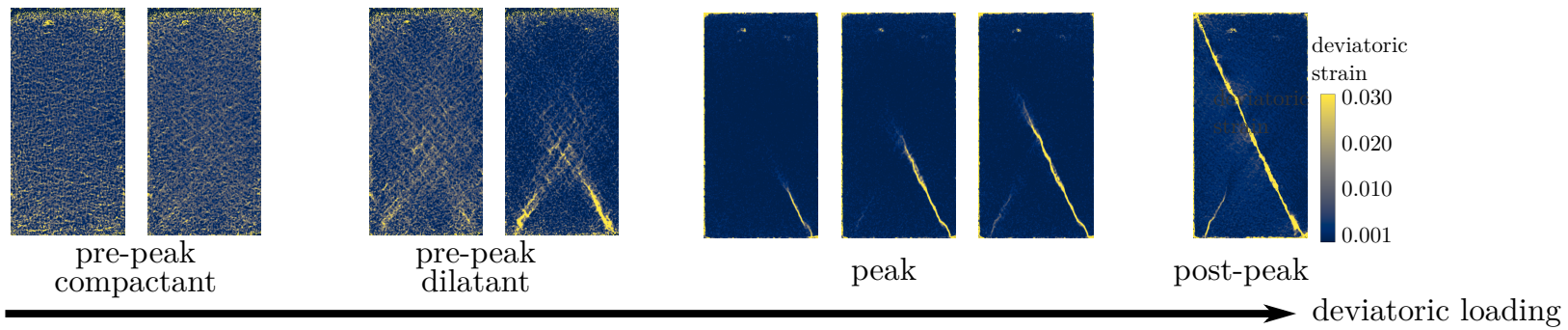

- Ductile behavior: at high mean stress and low Lode angle

  σ_m= 90 MPa, $\theta = 0^o$

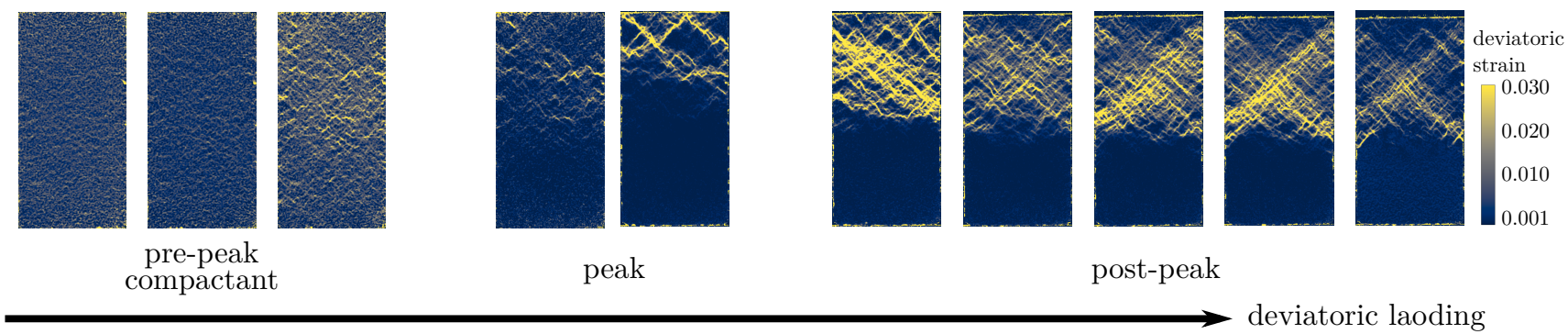

Three invariants failure surface

Linear-exponential function
(meridian plane)

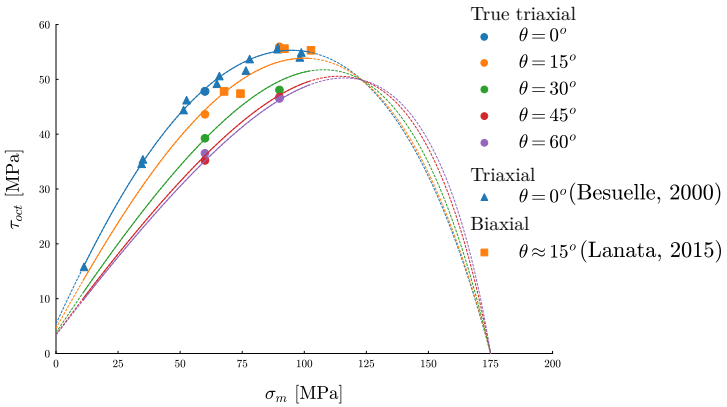

van-Eekelen function
(octahedral plane)

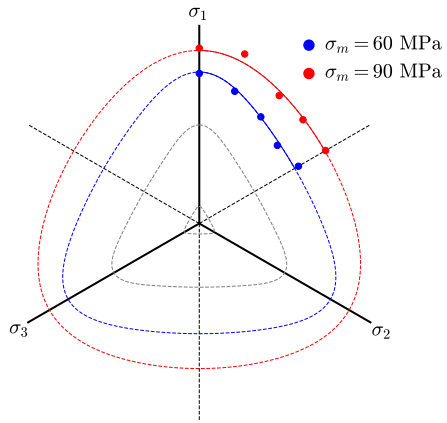

True triaxial experiments: bifurcation analysis

Three invariants failure surface

Linear-exponential function
(meridian plane)

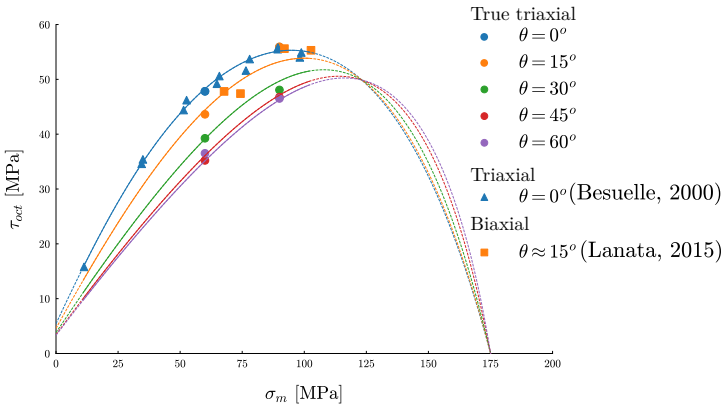

van-Eekelen function
(octahedral plane)

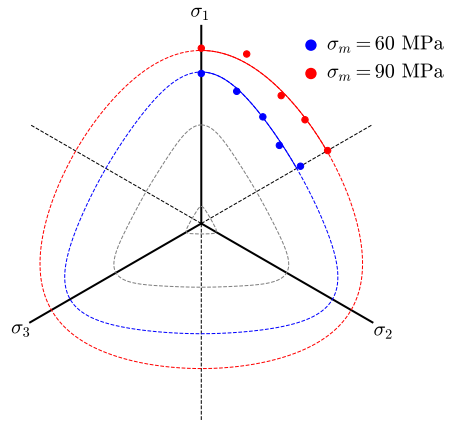

Prediction of mature deformation band kinematic for an elasto-plastic model

band angle in the 1-3 plane

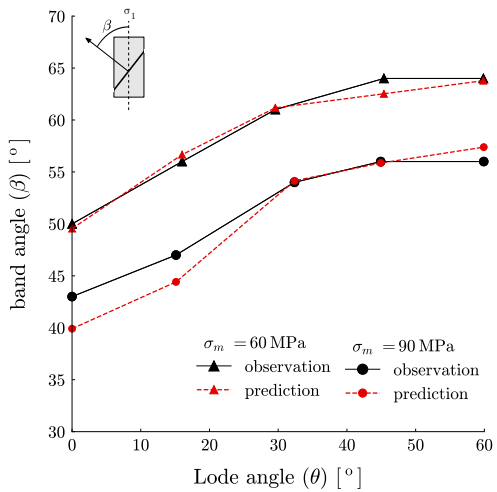

dilatancy angle

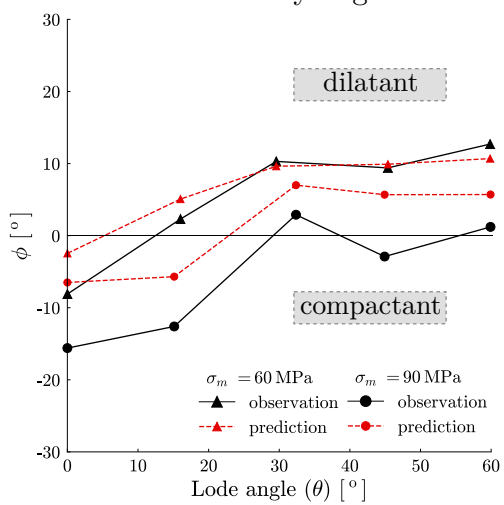

Model comparison

The three invariant model provides a better fit than simplified models:

deformation band angle

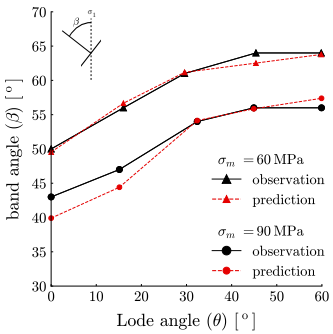

(a) initial model

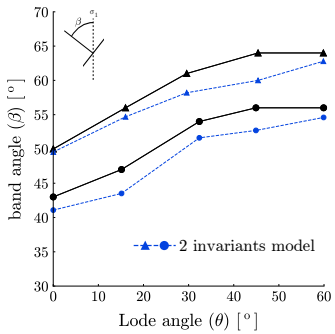

(b) 2 invariants model

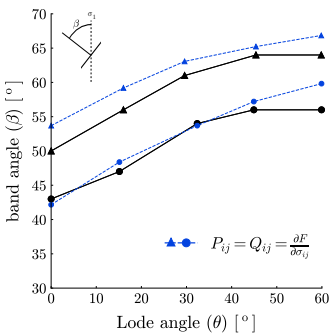

(c) associated model

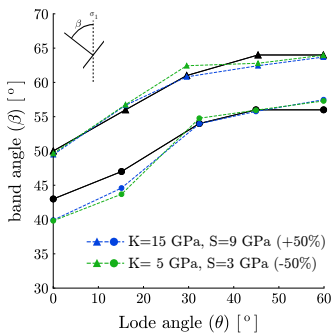

(d) elastic parameter sensitivity

dilatancy angle

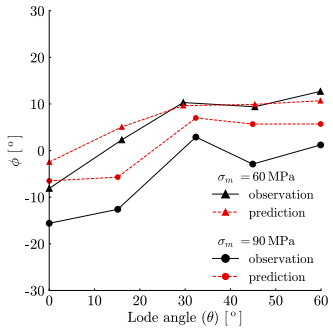

(a) initial model

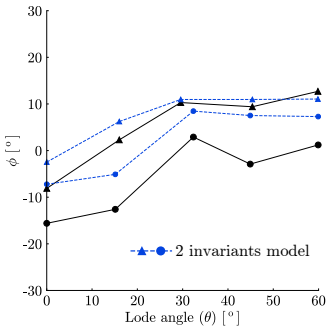

(b) 2 invariants model

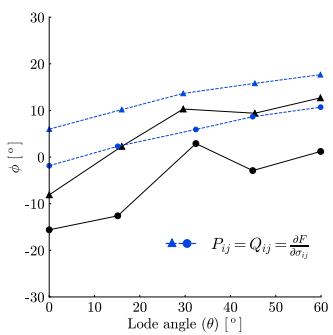

(c) associated model

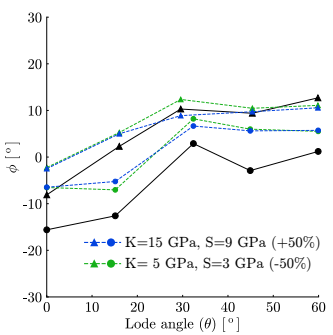

(d) elastic parameter sensitivity

Meridian plane: non-associated
Octahedral plane: associated

meridian plane

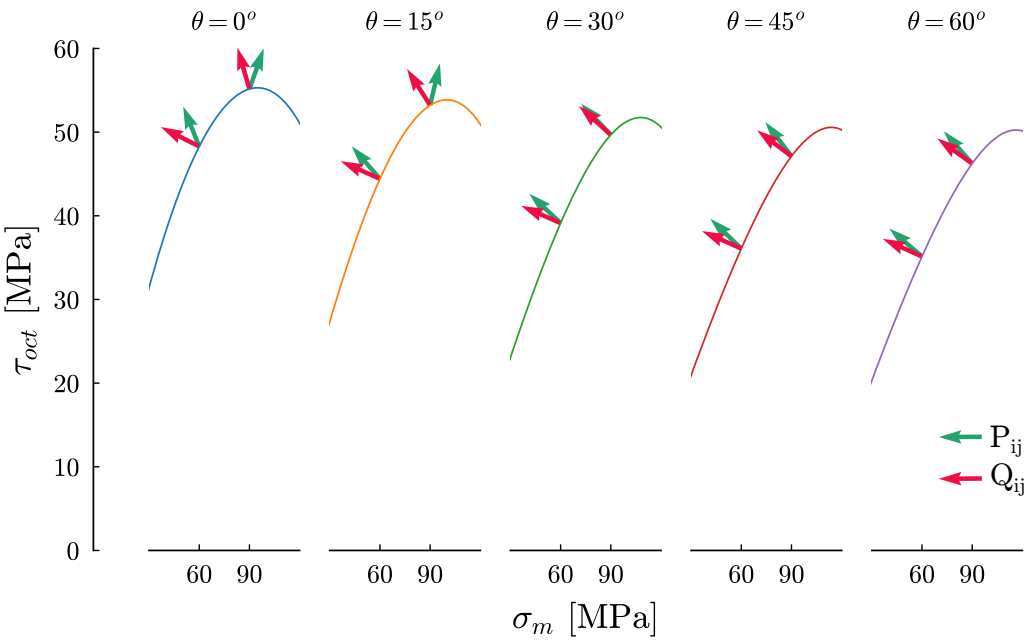

octahedral plane

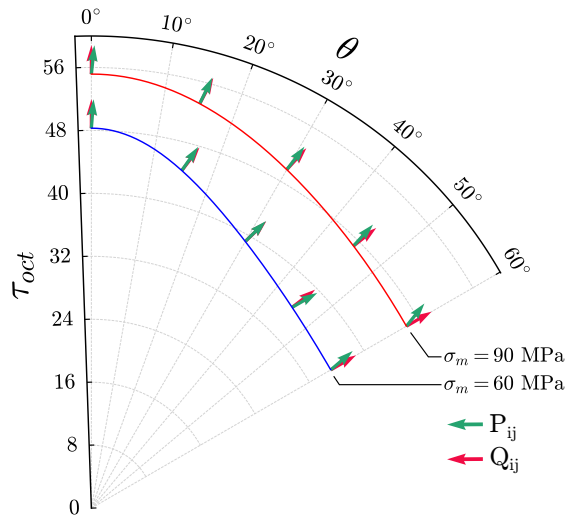

Anisotropic Vosges sandstone (23% average porosity)

Bedding plane anisotropy
with variable porosity

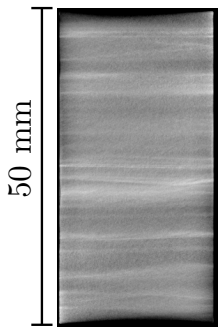

x-ray tomography
projection in 1-3 plane

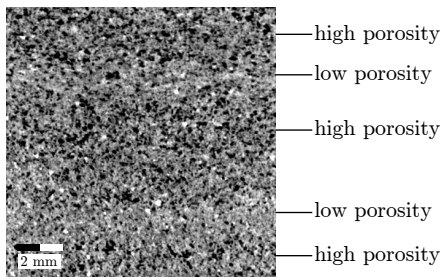

x-ray tomography
cross-section

Identical preparation to the isotropic sandstone

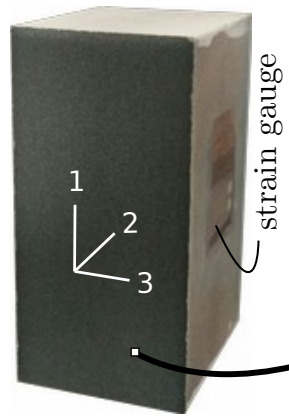

Speckled surface
400µm

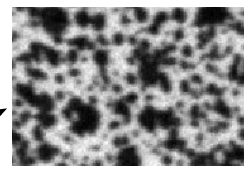

pixel size: 7µm/px

Anisotropic Vosges sandstone (23% average porosity)

Bedding plane anisotropy
with variable porosity

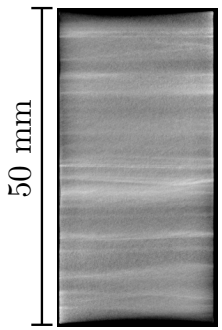

x-ray tomography
projection in 1-3 plane

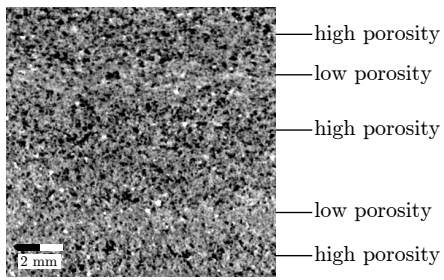

x-ray tomography
cross-section

Identical preparation to the isotropic sandstone

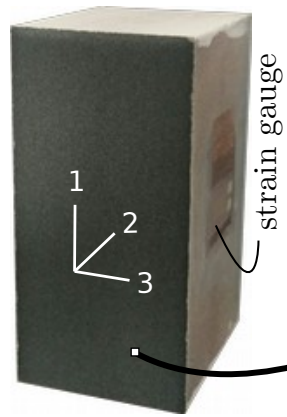

Speckled surface
400µm

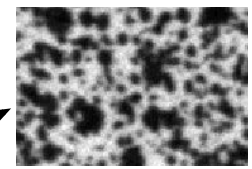

pixel size: 7µm/px

Experimental campaign on 21 samples

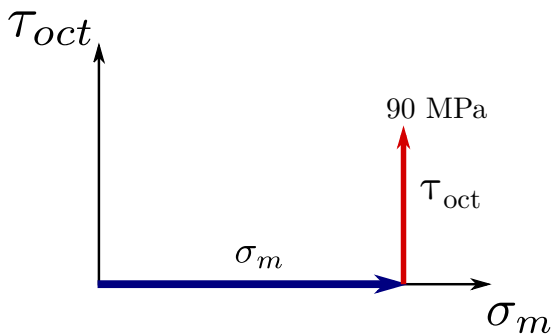

meridian plane (constant θ)

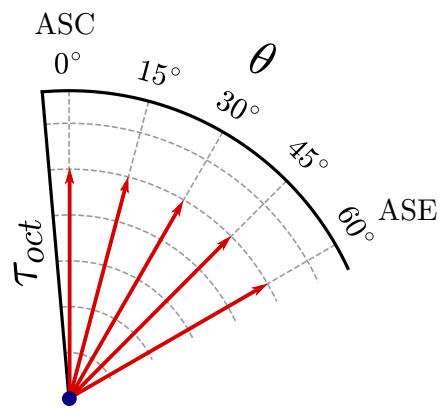

octahedral plane (constant σ_m)

Reconstructed tomography projected in a plane

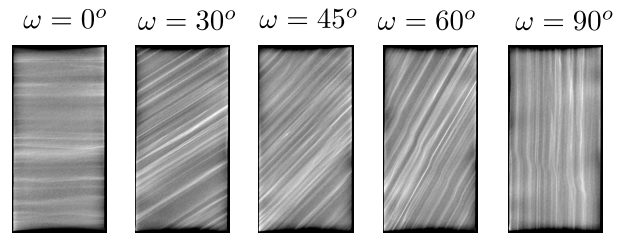

bedding plane angles in the 1-3 plane

True triaxial experiments: anisotropic sandstone

- Mature deformation bands independant of the bedding

$\omega = 30^o; \theta = 60^o$

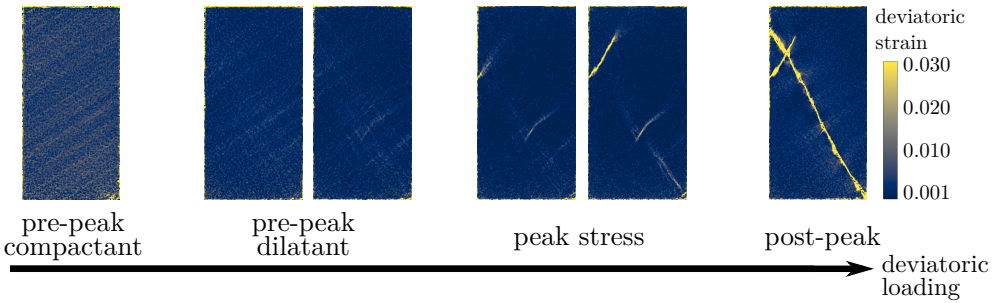

octahedral stress-strain curves

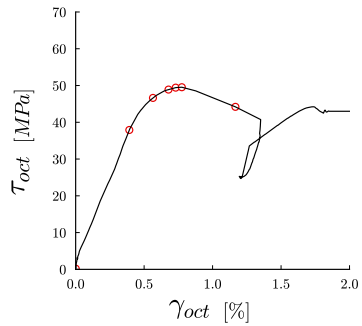

True triaxial experiments: anisotropic sandstone

Mature deformation bands independant of the bedding

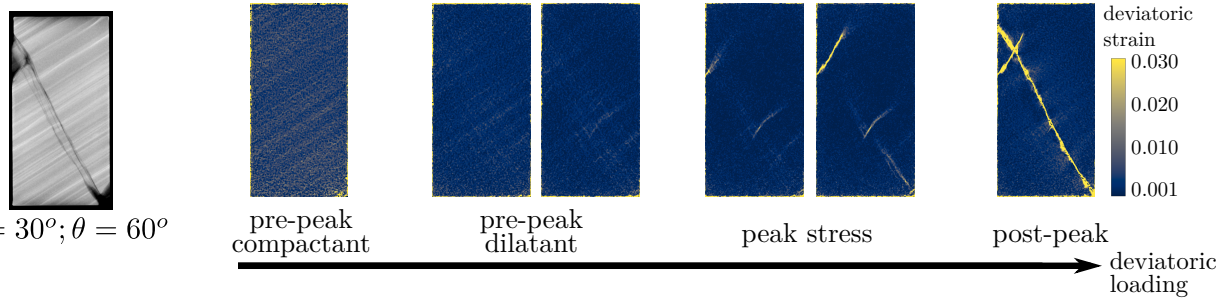

Mature deformation bands partially attracted by the bedding

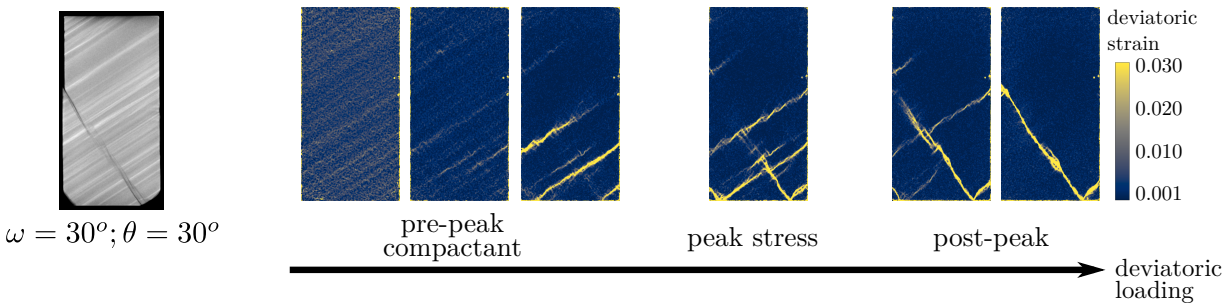

octahedral stress-strain curves

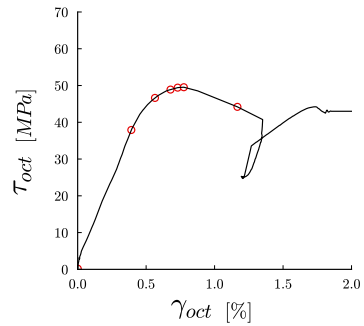

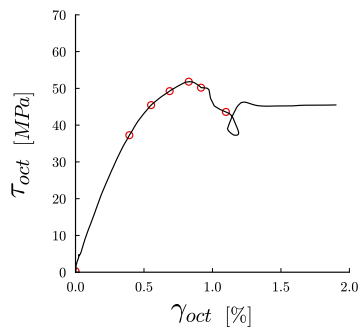

True triaxial experiments: anisotropic sandstone

Mature deformation bands independant of the bedding

$\omega = 30^o; \theta = 60^o$

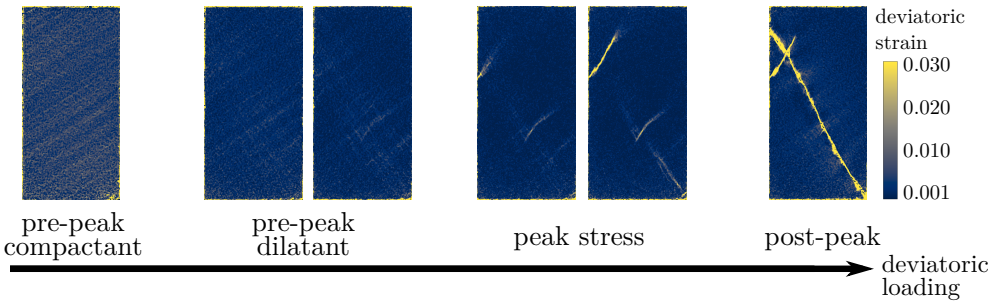

octahedral stress-strain curves

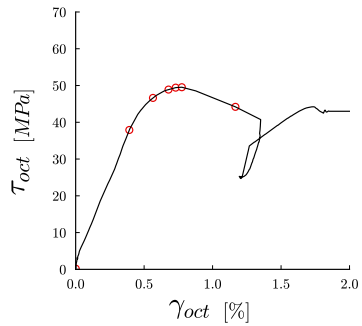

Mature deformation bands partially attracted by the bedding

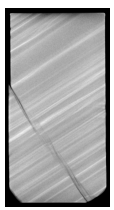

$\omega = 30^o; \theta = 30^o$

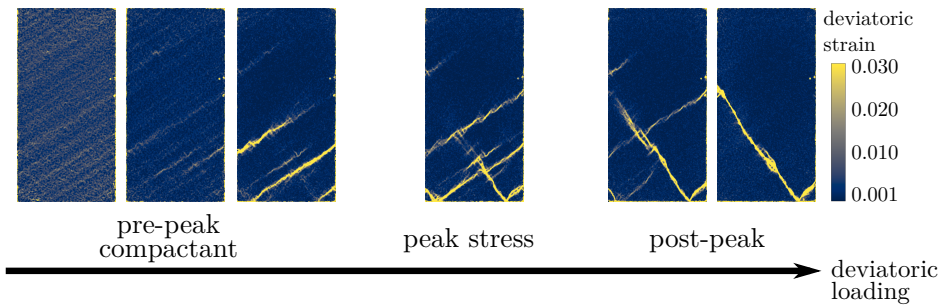

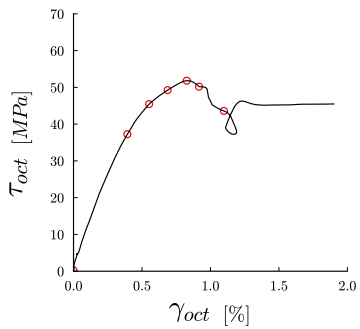

Mature deformation bands attracted by the bedding plane

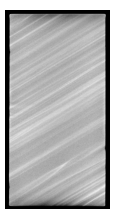

$\omega = 30^o; \theta = 0^o$

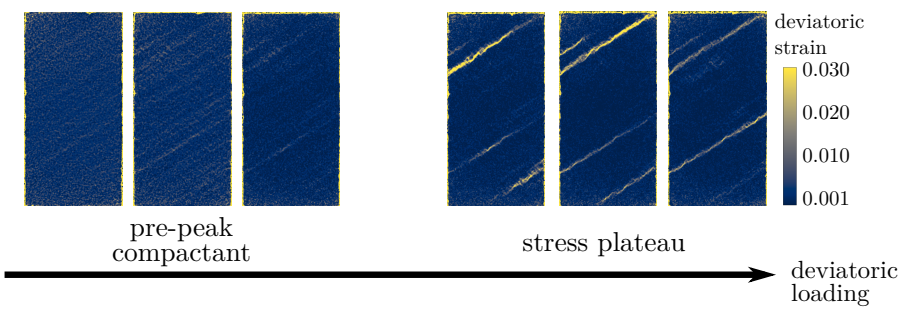

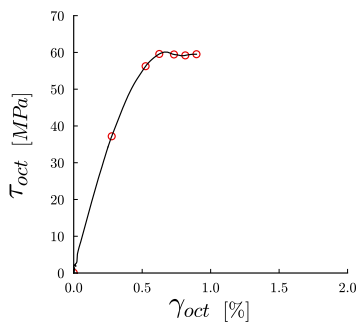

True triaxial experiments: anisotropic sandstone

Stress peak evolution
with the bedding plane angle

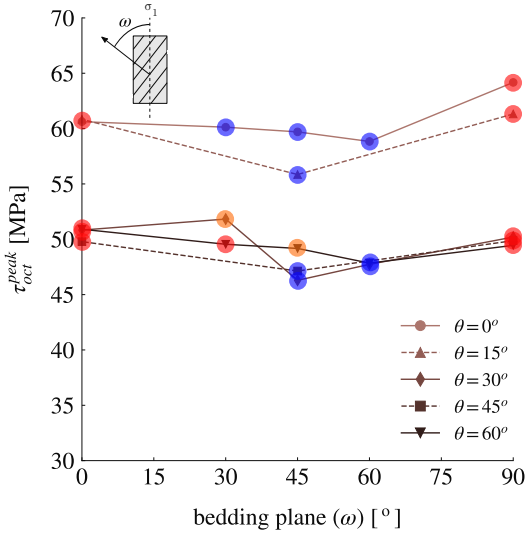

Deformation band angle evolution
with the bedding plane angle

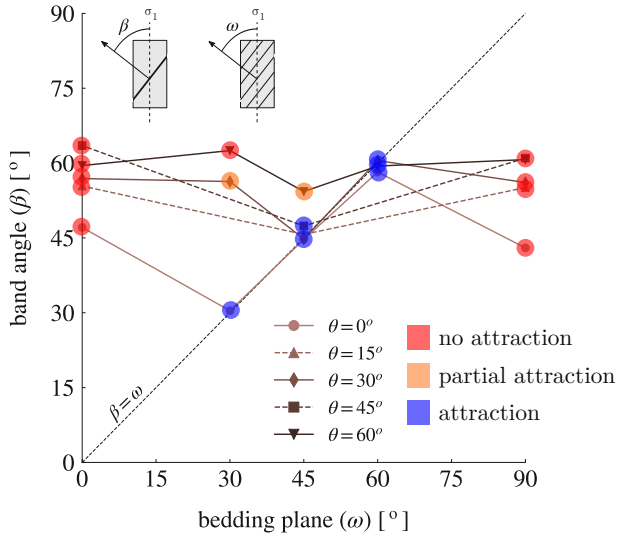

True triaxial experiments: anisotropic sandstone

Stress peak evolution
with the bedding plane angle

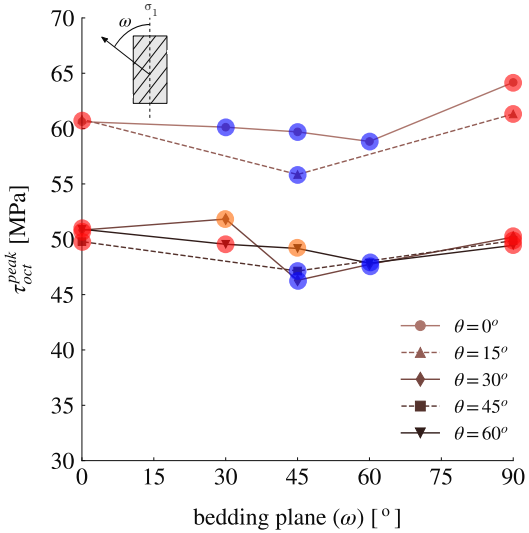

Deformation band angle evolution
with the bedding plane angle

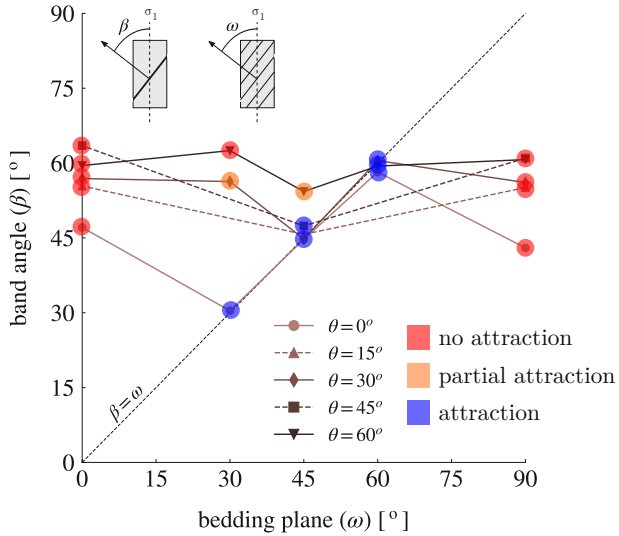

Comparable beahviour to rocks with pronounced bedding and lamination planes... but differs from typically observed strength anisotropy in sandstones

Green river shale [McLamore et al., 1967]

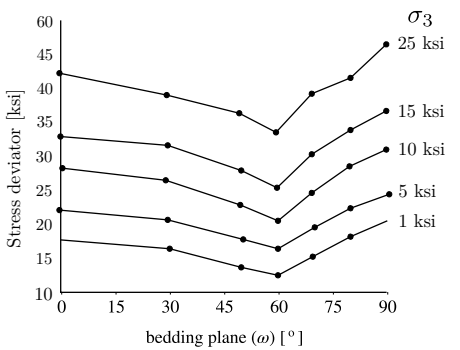

Adamwiller sandstone [Gatelier, 2002]

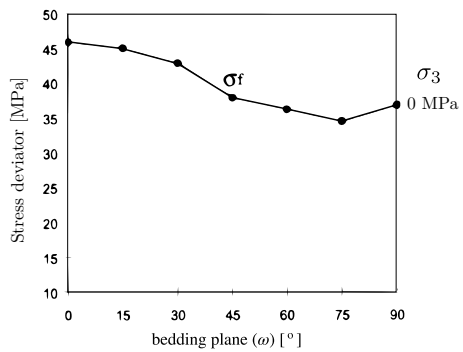

Adamwiller sandstone [Millien, 1993]

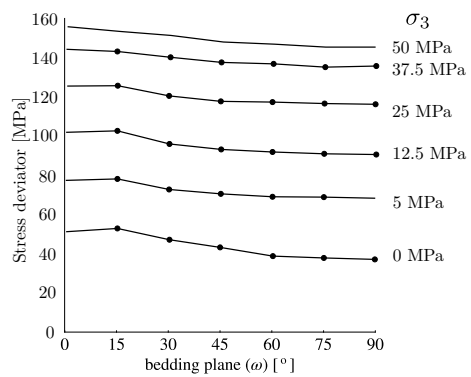

Macro scale | Micro scale

Rock matrix

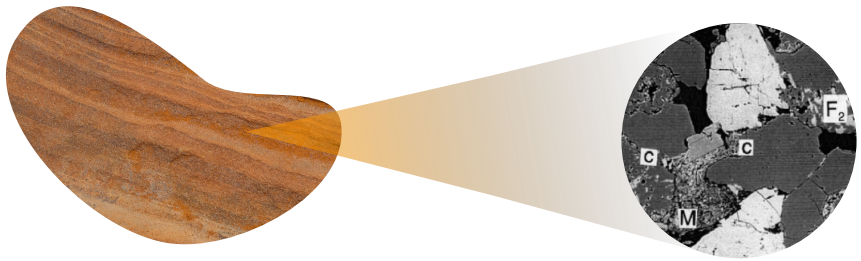

Granular assembly

FEM model

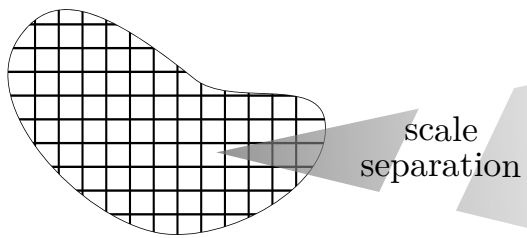

scale separation

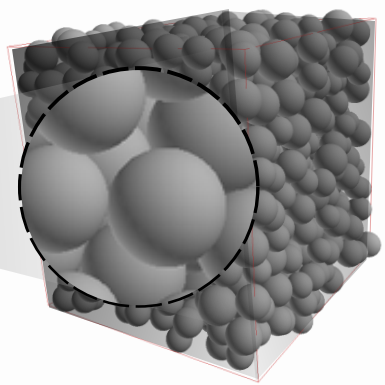

DEM model

Macro scale | Micro scale

Rock matrix

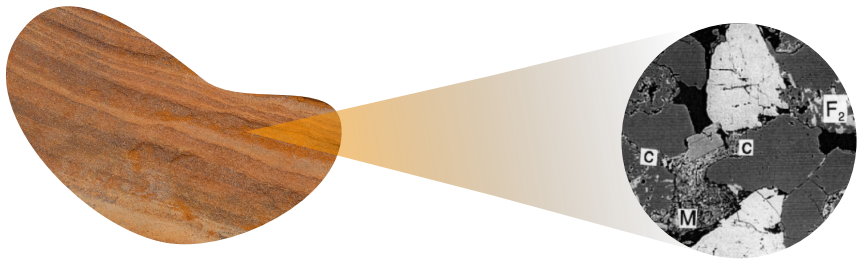

Granular assembly

FEM model

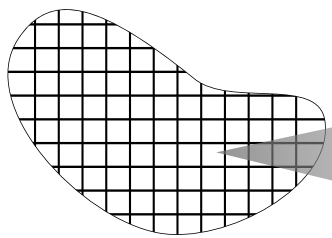

scale separation

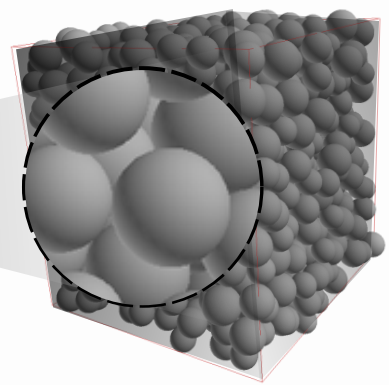

DEM model

NHL

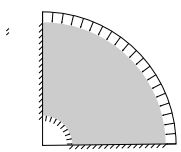

structure & boundary conditions

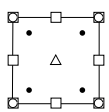

element

strain

stress

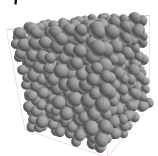

elementary volume

assembly

particle

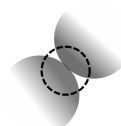

contact law

FEMxDEM simulations: concurrency and 2nd gradient model

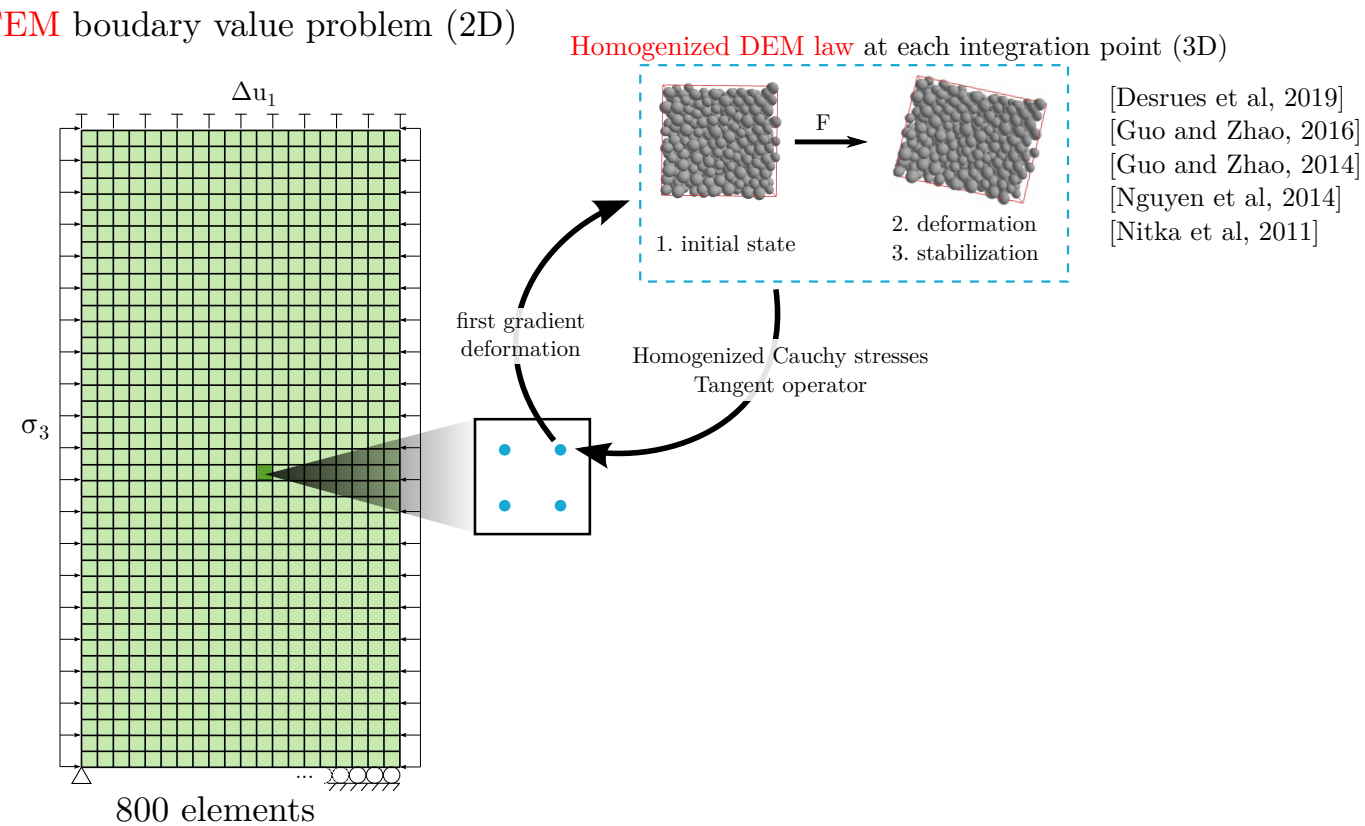

Numerical developments:

- True triaxial loading paths in 2D-3D to impose constant stress invariants
- Damageable cohesive-frictional contact law at the DEM level
- Random and organized distribution of elementary volumes at the integration points

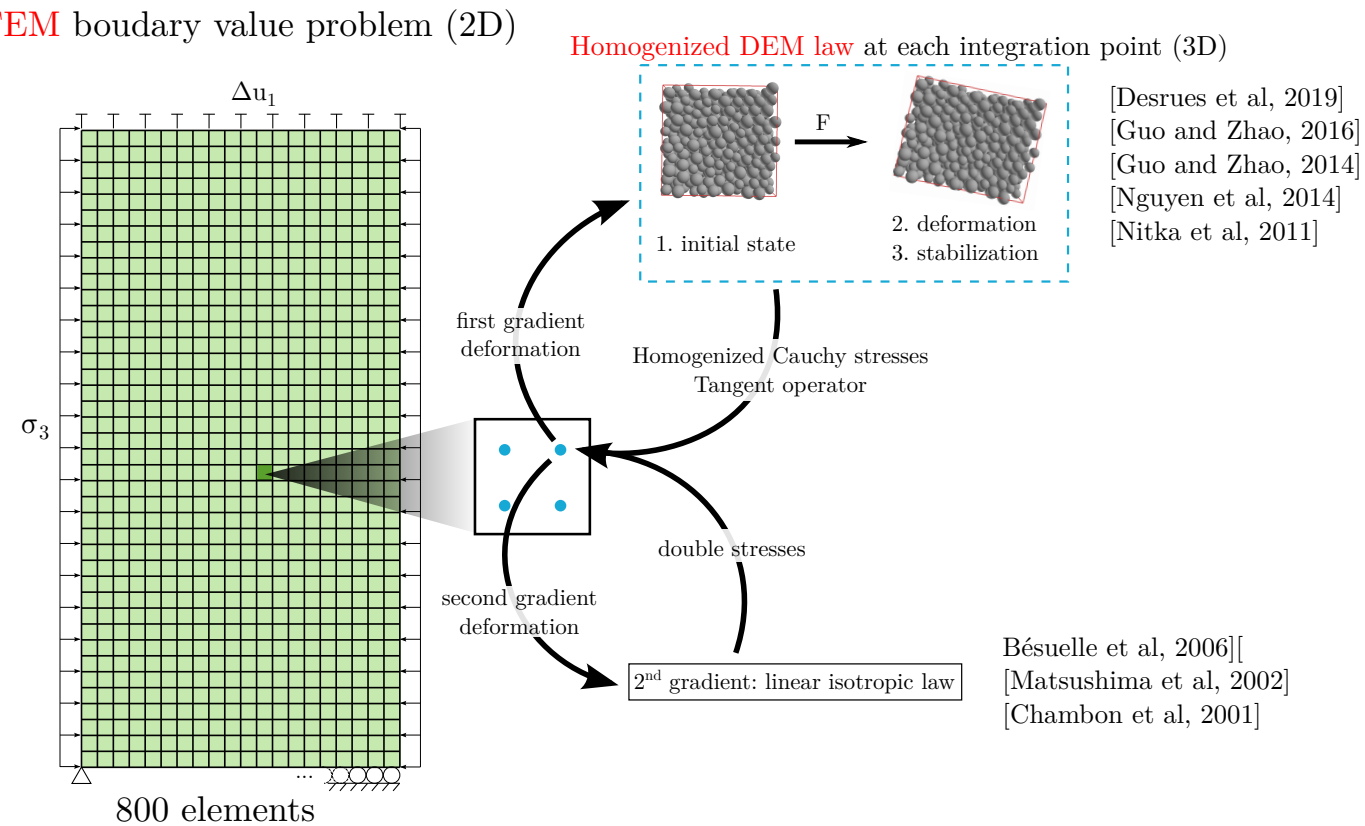

Numerical developments:

- True triaxial loading paths in 2D-3D to impose constant stress invariants
- Damageable cohesive-frictional contact law at the DEM level
- Random and organized distribution of elementary volumes at the integration points

Preparation of numerical samples:

- Three configurations of elementary volumes (EV): loose, dense and anisotropic

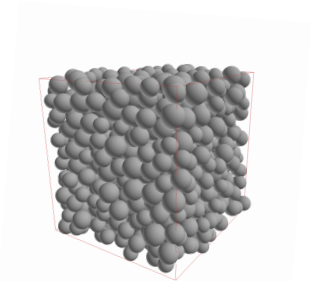

- 1000 spherical particles
- size distribtuion (r_{max}/r_{min}) = 1.4
- periodic boundary conditions
- identical contact law properties

	EV-1 (loose)	EV-2 (dense)	EV-3 (anisotropic)
Z	4.67	5.21	4.72
ϕ_{oct}	0.005	0.003	0.013
η (%)	40.1	38.9	39.4

Z : coordination number
ϕ_{oct} : fabric tensor second invariant

Preparation of numerical samples:

- Three configurations of elementary volumes (EV): loose, dense and anisotropic

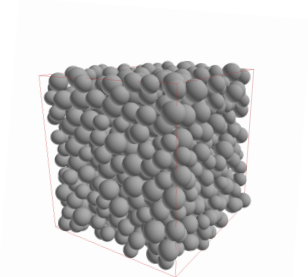

- 1000 spherical particles
- size distribtuion (r_{max}/r_{min}) = 1.4
- periodic boundary conditions
- identical contact law properties

	EV-1 (loose)	EV-2 (dense)	EV-3 (anisotropic)
Z	4.67	5.21	4.72
ϕ_{oct}	0.005	0.003	0.013
η (%)	40.1	38.9	39.4

Z : coordination number
ϕ_{oct} : fabric tensor second invariant

- Three case studies:

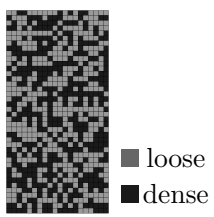

1. heterogeneous distribution dense and loose EV

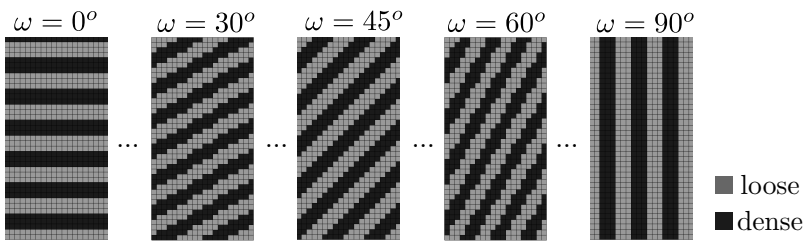

2. organized distribution in bedding planes of EV-1 and EV-2 (thickness of 3 elements)

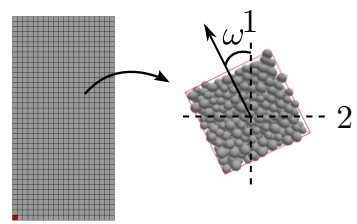

3. homogeneous distribution of rotated anisotropic EV-3

Heterogeneous distribution of elementary volumes: influence of the Lode angle

Octahedral stress peak

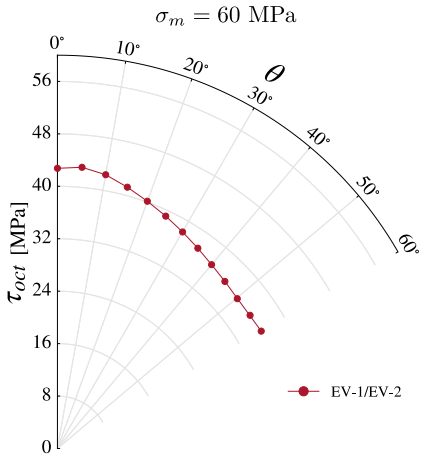

Deformation band angle

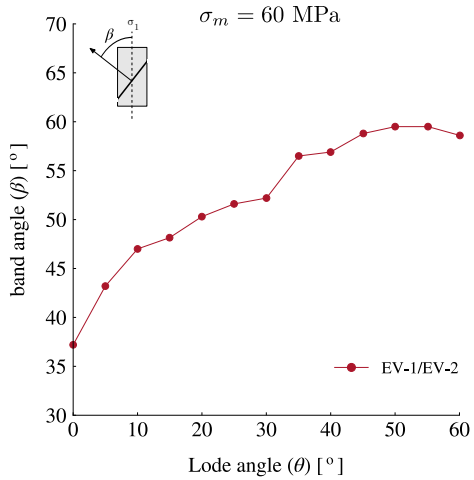

Incremental deformation field

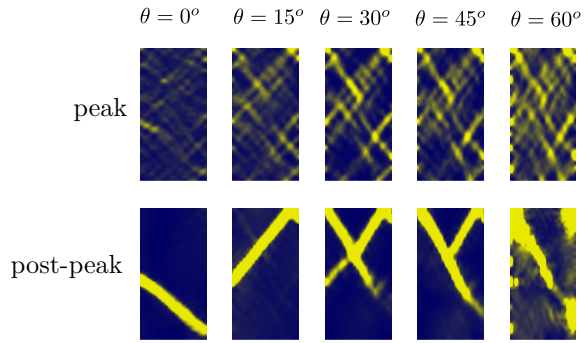

Heterogeneous distribution of elementary volumes: influence of the Lode angle

Octahedral stress peak

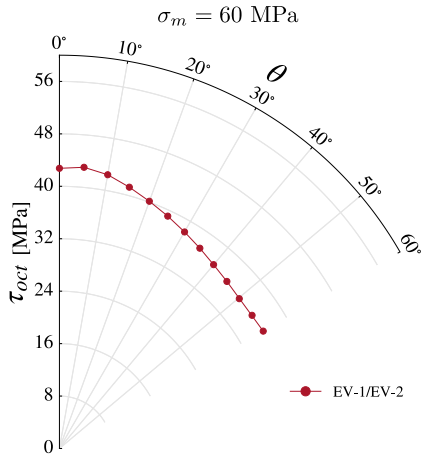

Deformation band angle

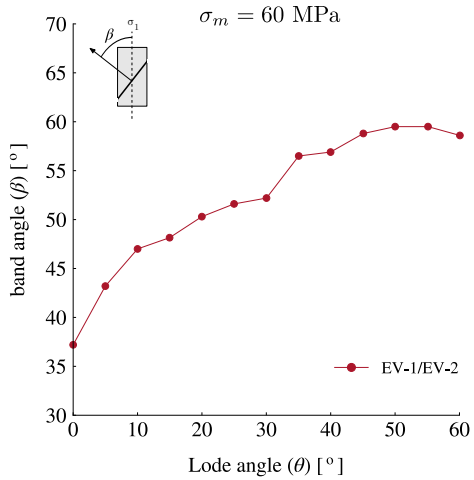

Incremental deformation field

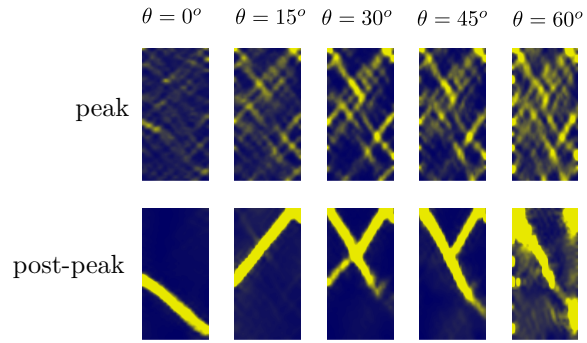

- Comparison with experimental observations (isotropic sandstone)

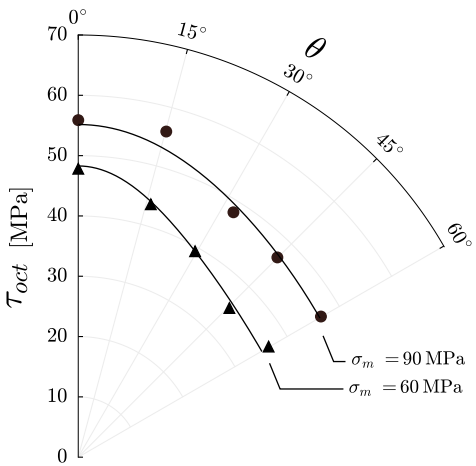

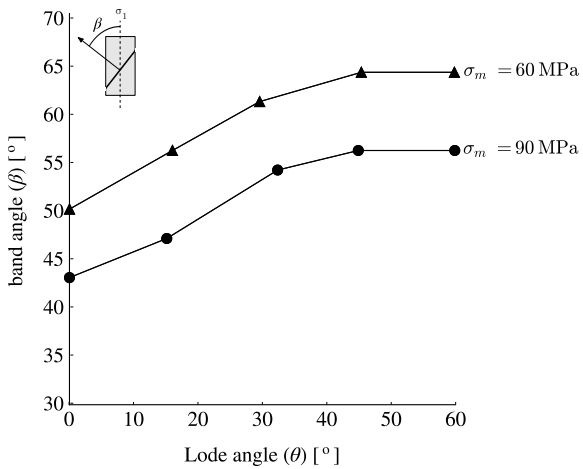

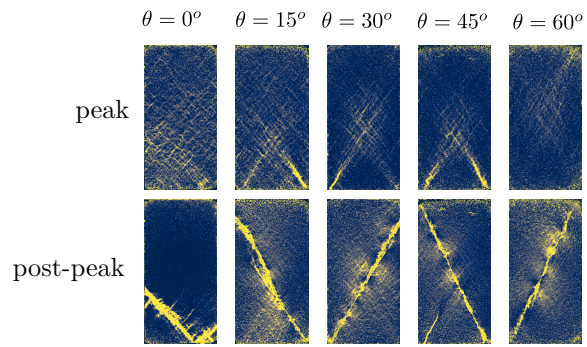

Distribution of elementary volumes in bedding planes: effect of the bedding plane angle

Octahedral stress peak

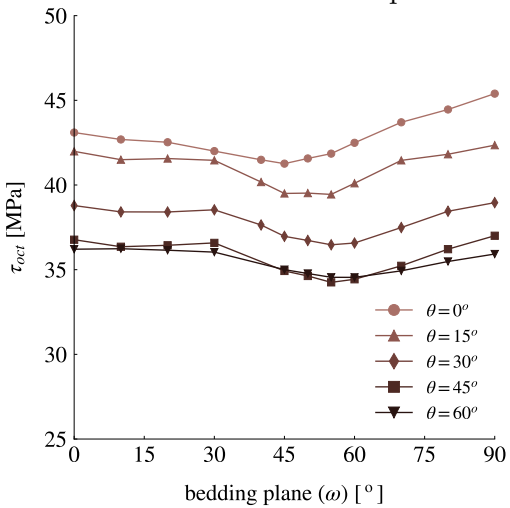

Deformation band angle

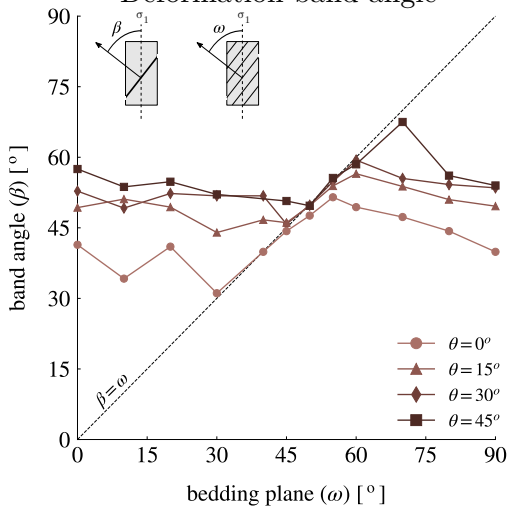

Incremental deformation field

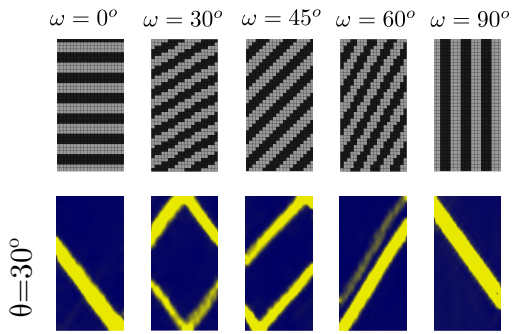

Distribution of elementary volumes in bedding planes: effect of the bedding plane angle

Octahedral stress peak

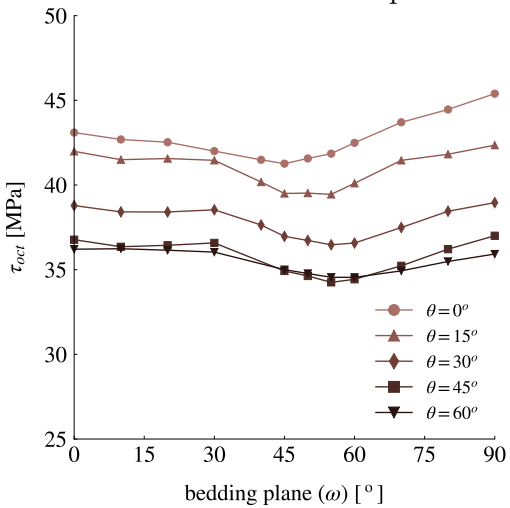

Deformation band angle

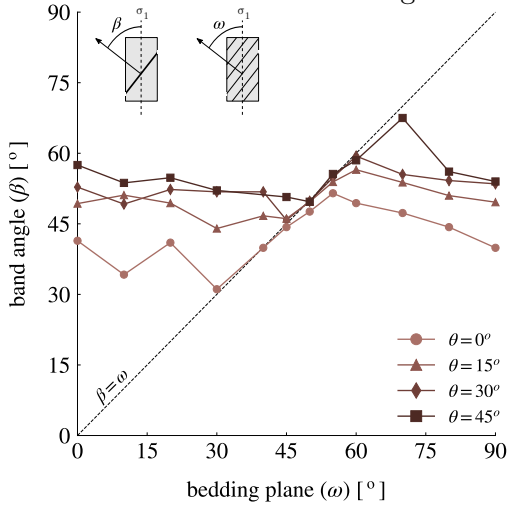

Incremental deformation field

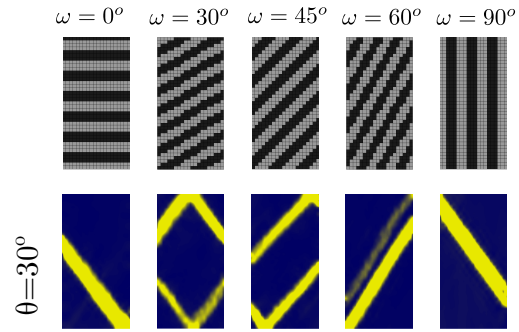

- Comparison with experimental observations (anisotropic sandstone)

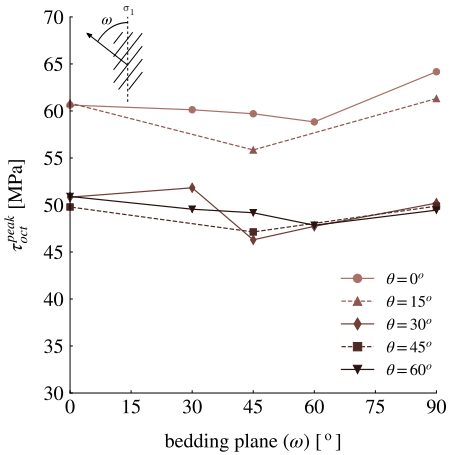

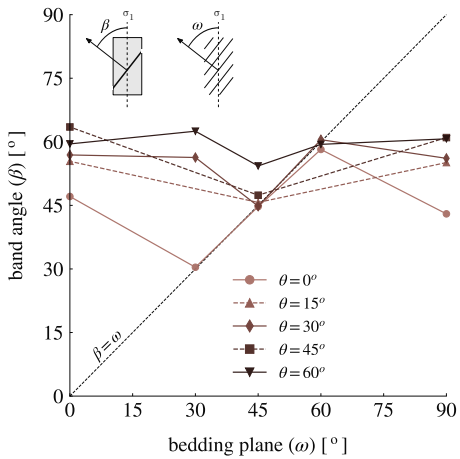

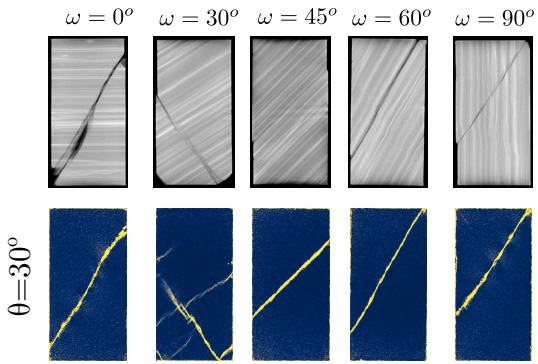

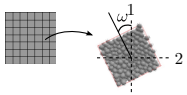

Rotation of anisotropic elementary volumes with respect to imposed principal stresses

Pic de contrainte

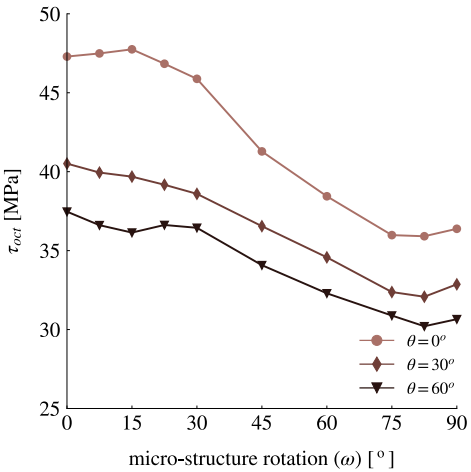

Angle des bandes de déformation

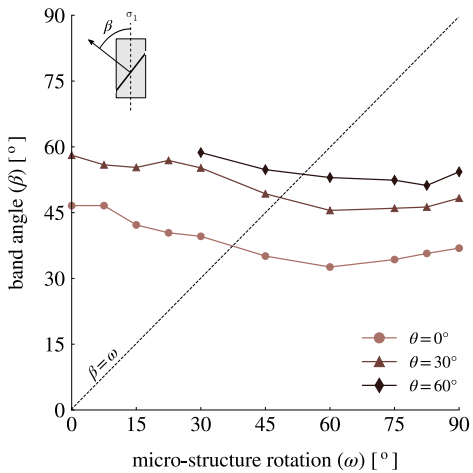

FEMxDEM simulations of sandstone

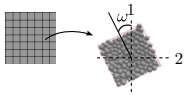

Rotation of anisotropic elementary volumes with respect to imposed principal stresses

Pic de contrainte

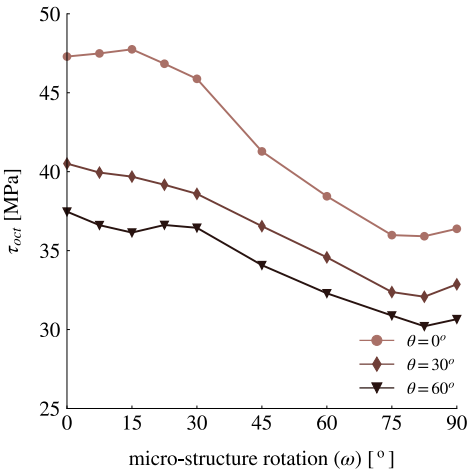

Angle des bandes de déformation

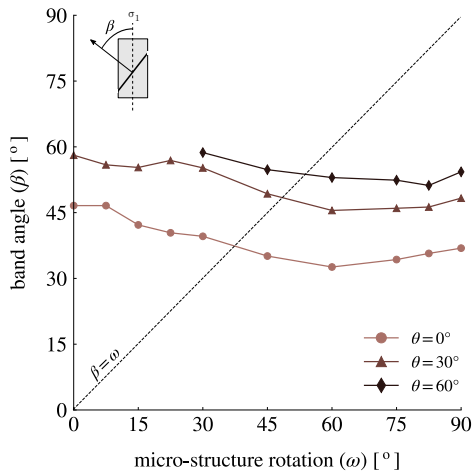

- Comparison with data from the litterature (anisotropic sandstone)

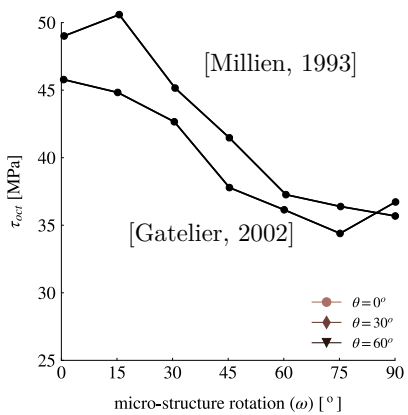

Adamwiller sandstone
Uniaxial loading

Contributions

Experimental study

- Experimental procedure using a true triaxial apparatus with invariants controlled loading paths and full-field measurements
- Experimental campaigns on istropic and anisotropic sandstones highlighing: localization transitions in the brittle-ductile regime, role of the Lode angle, emergence of early deformation bands, effect of bedding plane anisotropy, ...

Contributions

Experimental study

- Experimental procedure using a true triaxial apparatus with invariants controlled loading paths and full-field measurements
- Experimental campaigns on istropic and anisotropic sandstones highlighing: localization transitions in the brittle-ductile regime, role of the Lode angle, emergence of early deformation bands, effect of bedding plane anisotropy, ...

Theoretical study

- Bifurcation analysis for a three invariants model, showing a good agreement between observations and prediction of deformation band kinematic

Contributions

Experimental study

- Experimental procedure using a true triaxial apparatus with invariants controlled loading paths and full-field measurements
- Experimental campaigns on istropic and anisotropic sandstones highlighing: localization transitions in the brittle-ductile regime, role of the Lode angle, emergence of early deformation bands, effect of bedding plane anisotropy, ...

Theoretical study

- Bifurcation analysis for a three invariants model, showing a good agreement between observations and prediction of deformation band kinematic

Numerical study

- Damageable cohesive-frictional contact law and loading path procedure for a double scale FEMxDEM model
- Numerical simulations on the effect of true triaxial loading path for heterogeneous rocks and material anisotropy at different scales

Acknowledgments

My thesis supervisors

Pierre Bésuelle and **Jacques Desrues**

Experimental contributions

spam developers and in particular **Edward Ando**, **Olga Stamati** and **Denis Caillerie**

Numerical contributions

Vincent Richefeu and **Frédéric Collin**

Unsorted contributions

Patrick Selvadurai and **Cino Viggiani**

Acknowledgments

My thesis supervisors

Pierre Bésuelle and **Jacques Desrues**

Experimental contributions

spam developers and in particular **Edward Ando**, **Olga Stamati** and **Denis Caillerie**

Numerical contributions

Vincent Richefeu and **Frédéric Collin**

Unsorted contributions

Patrick Selvadurai and **Cino Viggiani**

Thanks to the members of the jury and the ALERT community

Deviatoric strain field at peak stress

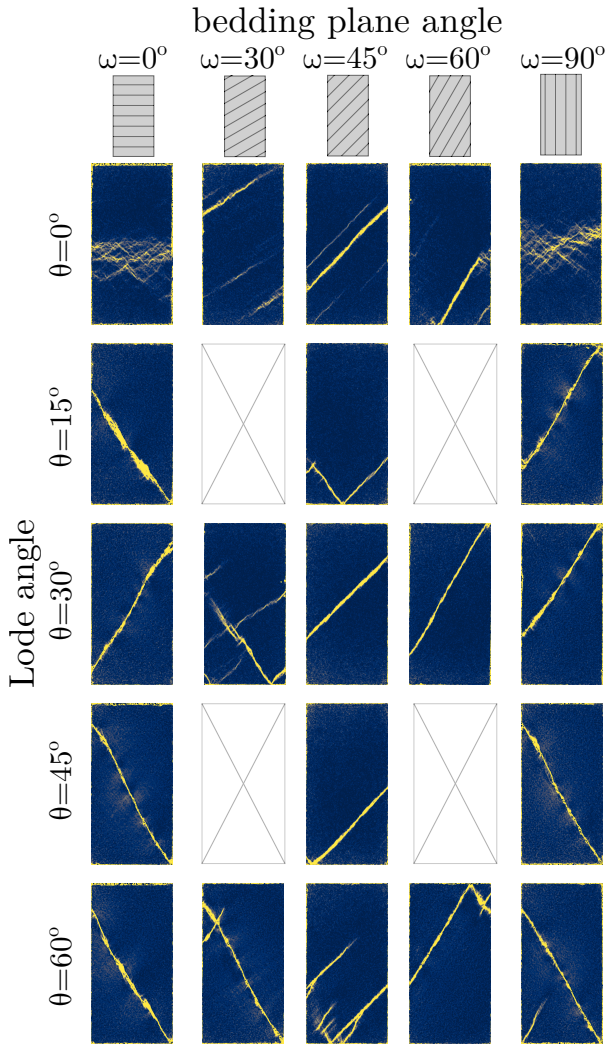

Reconstructed tomography projected in a plane

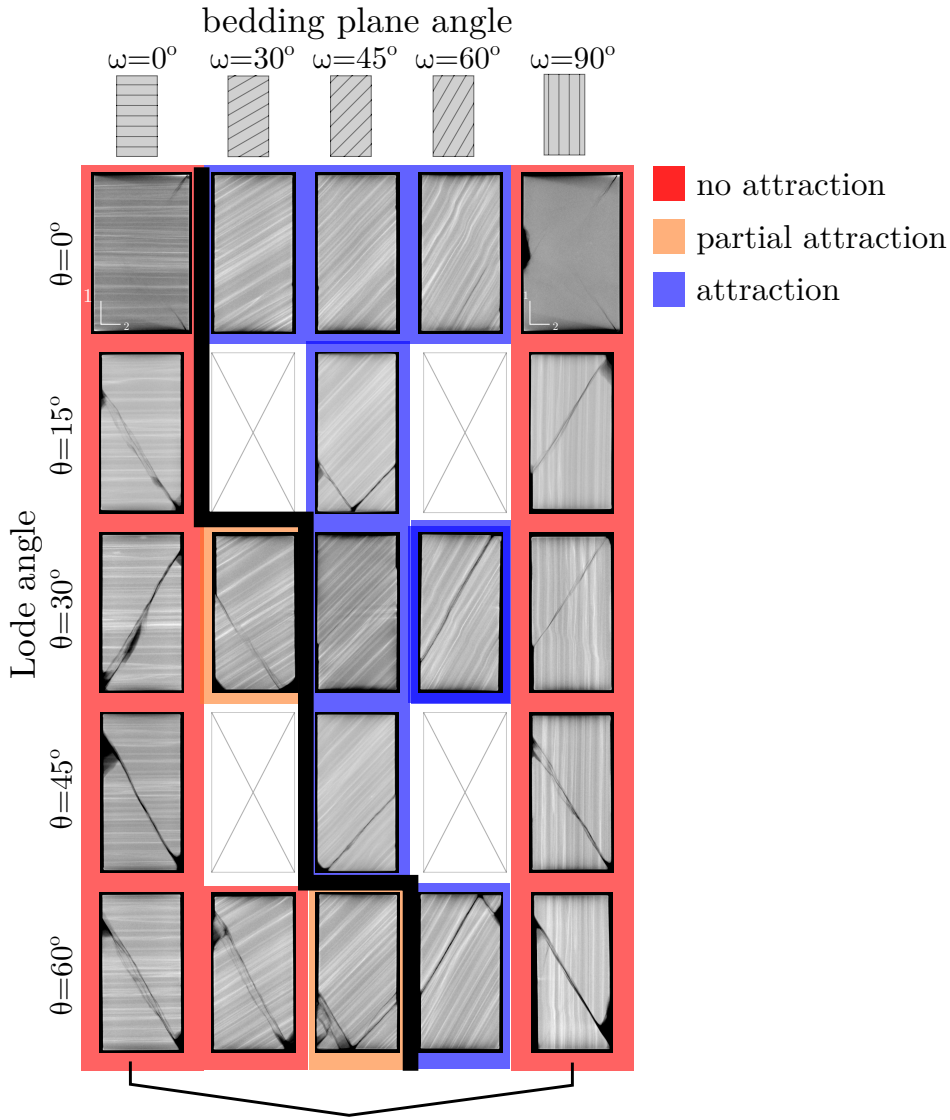

influence of the Lode angle similar to the isotropic sandstone

Deformation band cross section

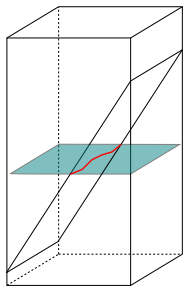

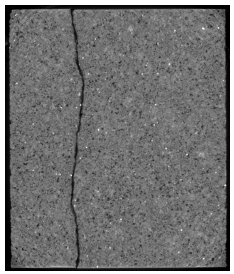

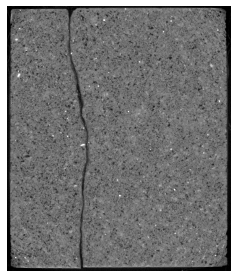

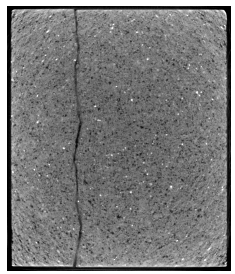

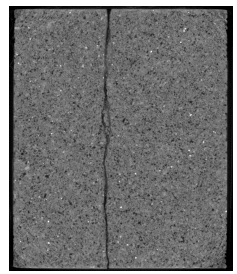

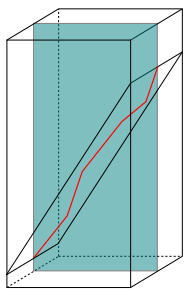

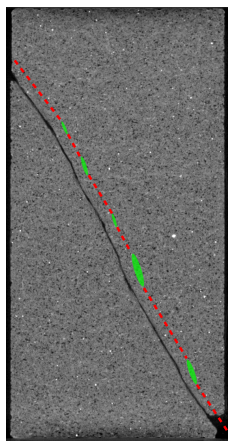

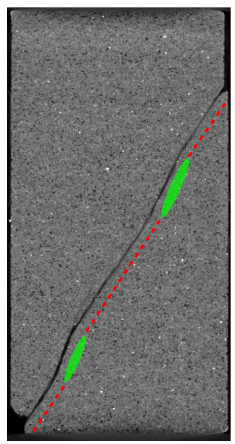

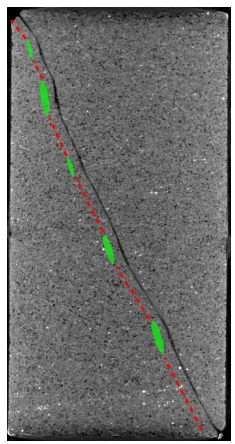

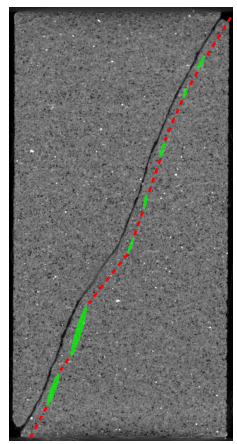

Deformation band profile

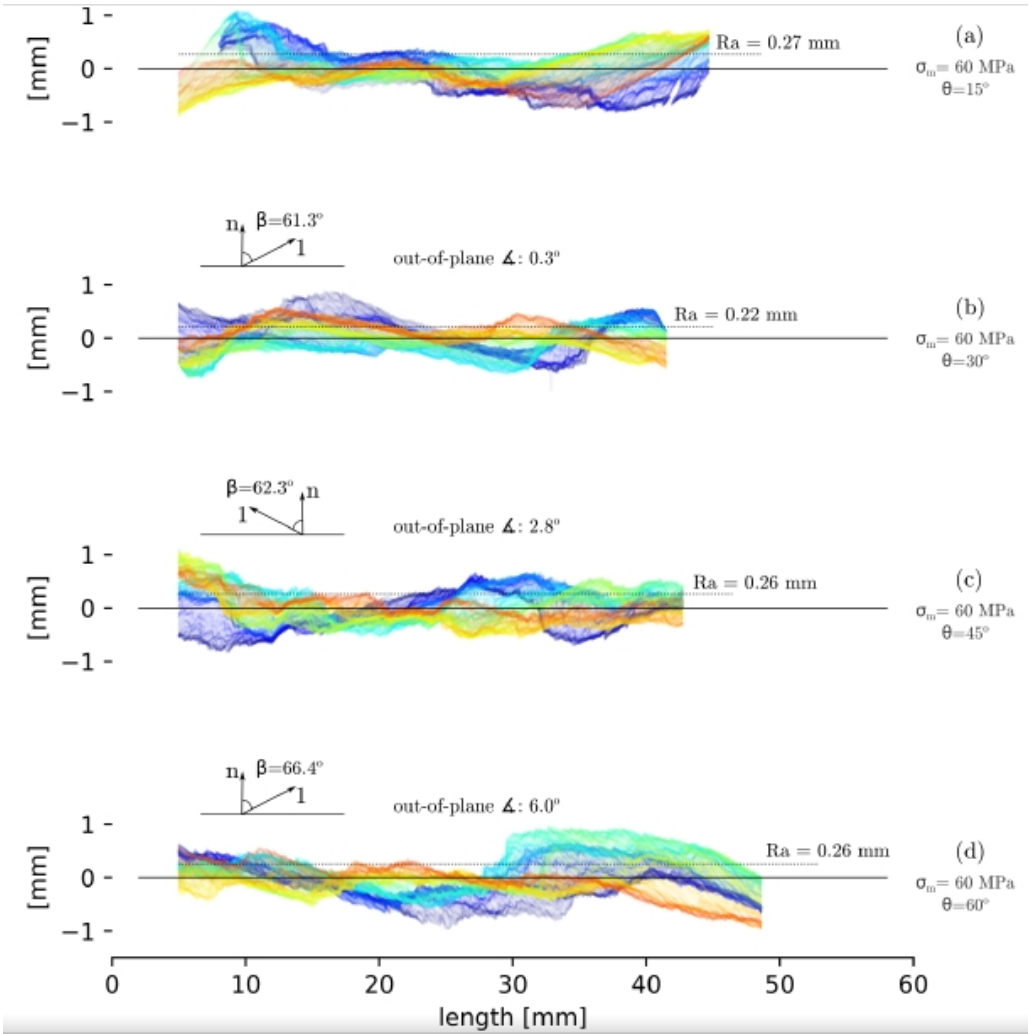

Failure surface in the meridian plane

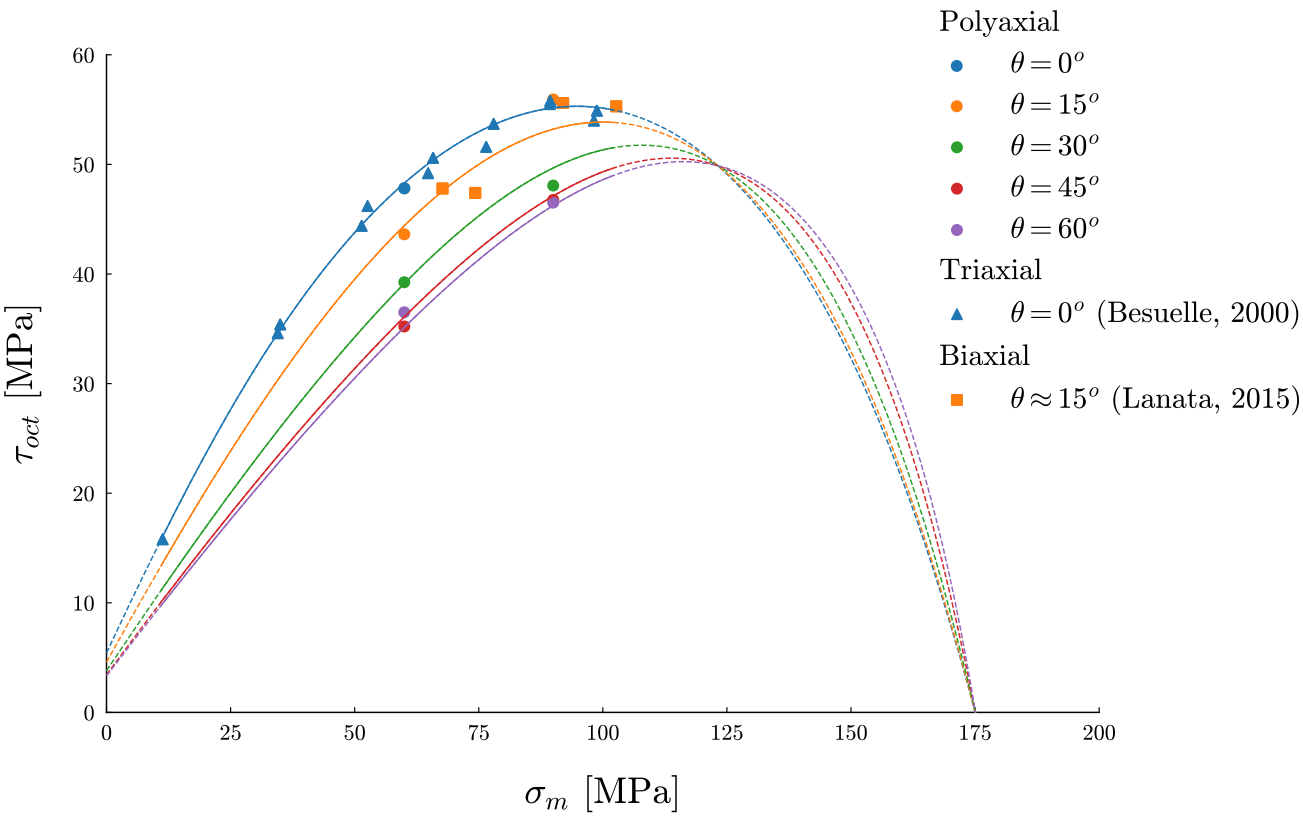

Failure surface in the octahedral plane

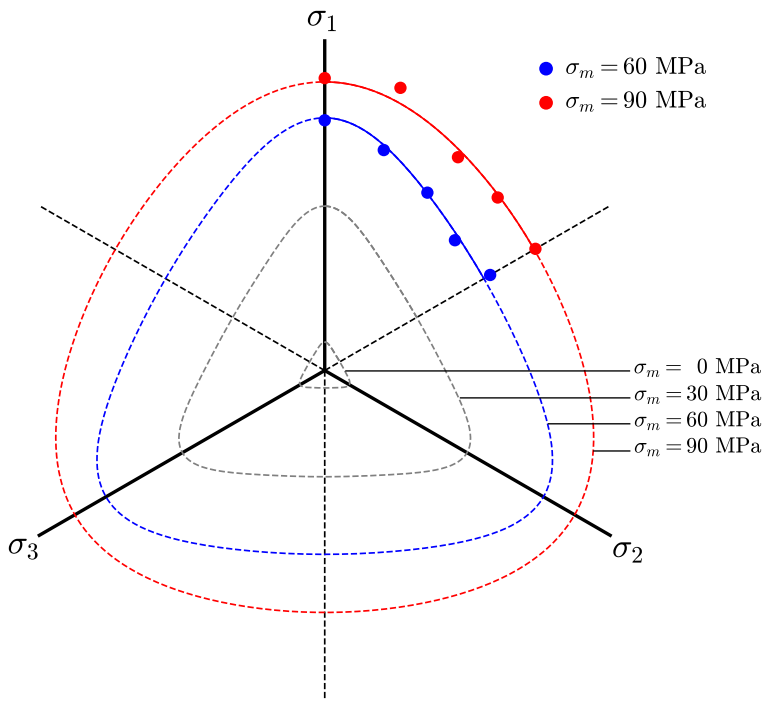

(a) $F_\sigma > 0$

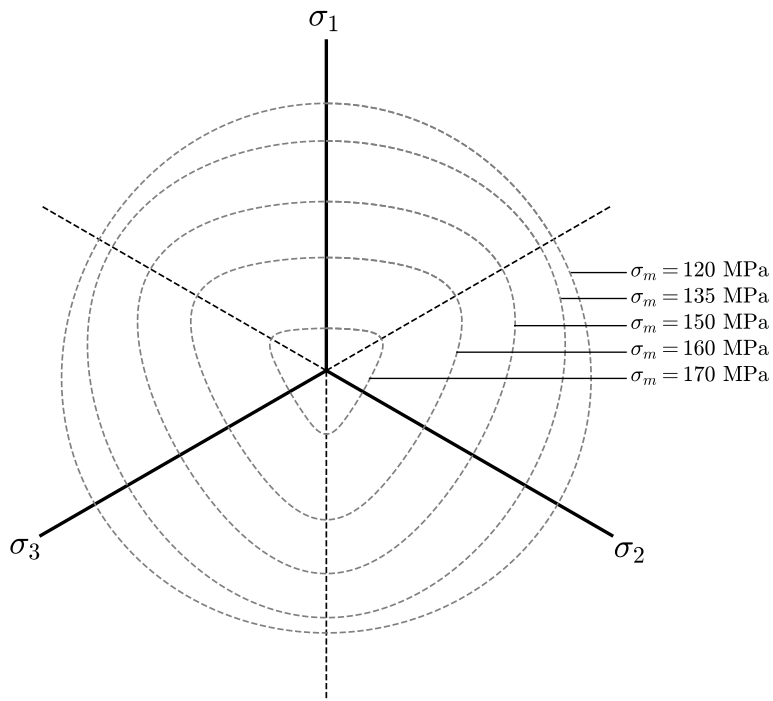

(b) $F_\sigma < 0$

Directions of P and Q

meridian plane

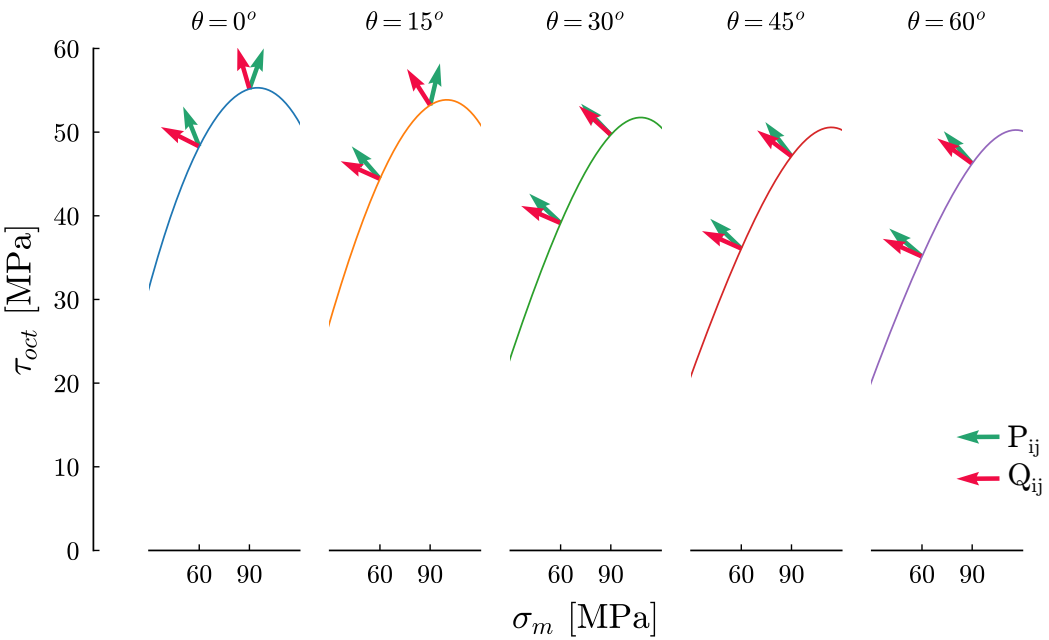

octahedral plane

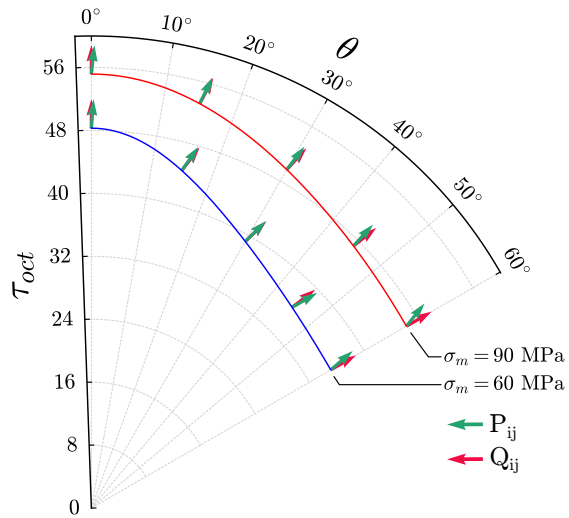

Bifurcation criteria

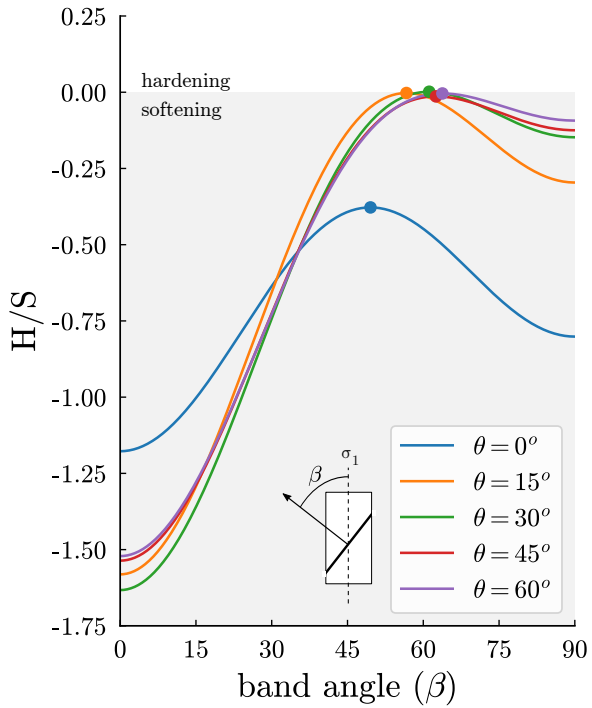

(a) $\sigma_m = 60$ MPa

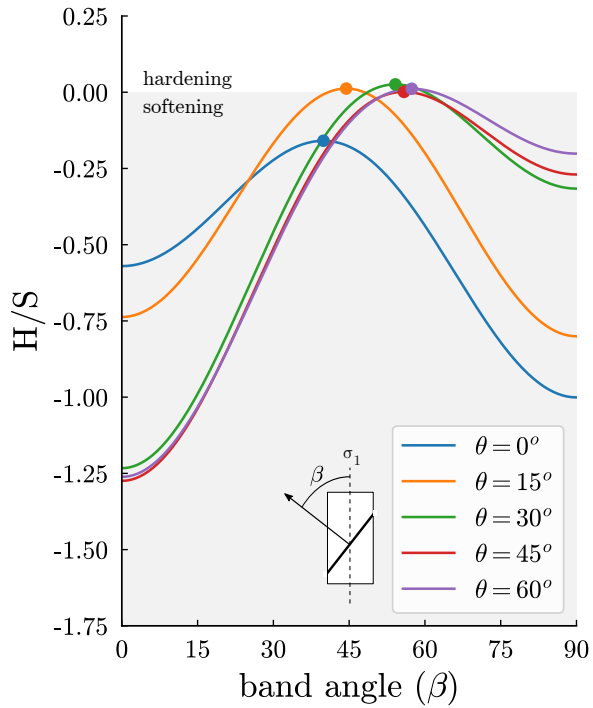

(b) $\sigma_m = 90$ MPa

Model comparison

band angle

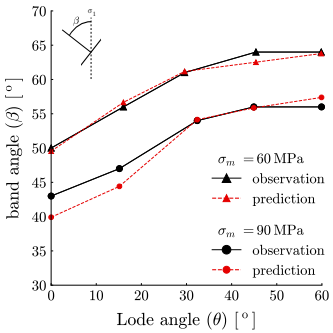

(a) initial model

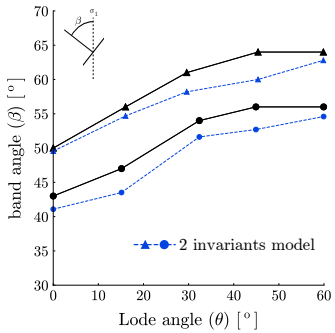

(b) 2 invariants model

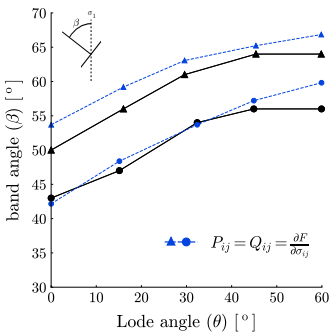

(c) associated model

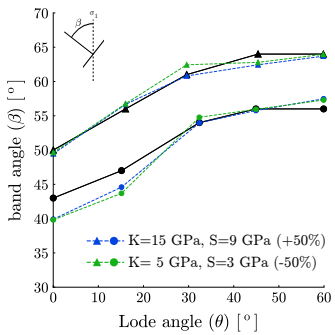

(d) elastic parameter sensitivity

dilatancy angle

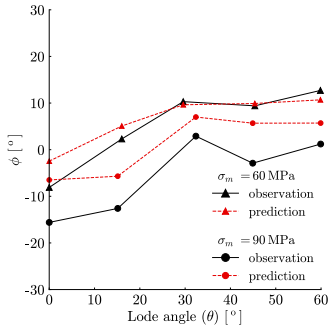

(a) initial model

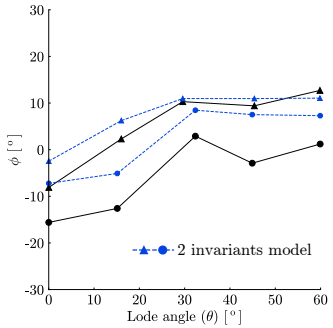

(b) 2 invariants model

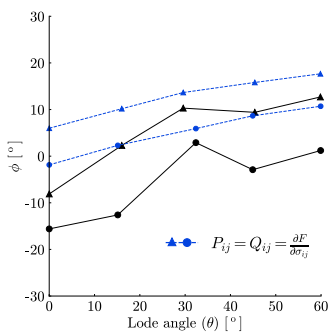

(c) associated model

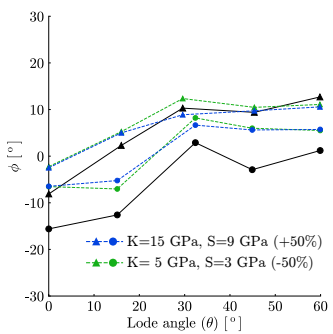

(d) elastic parameter sensitivity

DEM parameters

time step (Δt)	6.8×10^{-9} s
critical time step (t_c)	6.8×10^{-8} s
Particles	
radius ($a_{min} - a_{max}$)	250-350 μm
density (ρ)	2700 kg/m^3
Granular frictional law	
K_n^{gran}	10 KN/m
K_t^{gran}/K_n^{gran}	1
μ	0.5
Cohesive damageable law	
K_n^{coh}	10 KN/m
K_t^{coh}/K_n^{coh}	1
δ_n^0	2.5 μm
δ_t^0/δ_n^0	1
α	4
$\chi^\star$	1.2
Dimensionless numbers	
κ (at $\sigma_m = 20$ MPa)	1666
I	10^{-4}

DEM elementary volumes

	EV-1 (loose)	EV-2 (dense)	EV-3 (anisotropic)
μ_{ini}	0.2	0.1	0.2
ε_{ini}	0	0	5%
Z	4.67	5.21	4.72
Z^{coh}	3.73	4.16	3.77
$\eta(\%)$	40.1	38.9	39.4
ϕ_{oct}	0.005	0.003	0.013

Poisson sphere sampling

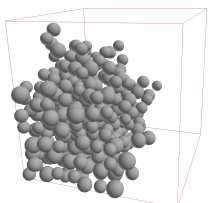

cohesion distribution

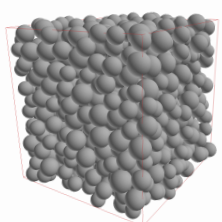

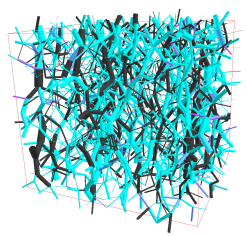

biaxial simulation

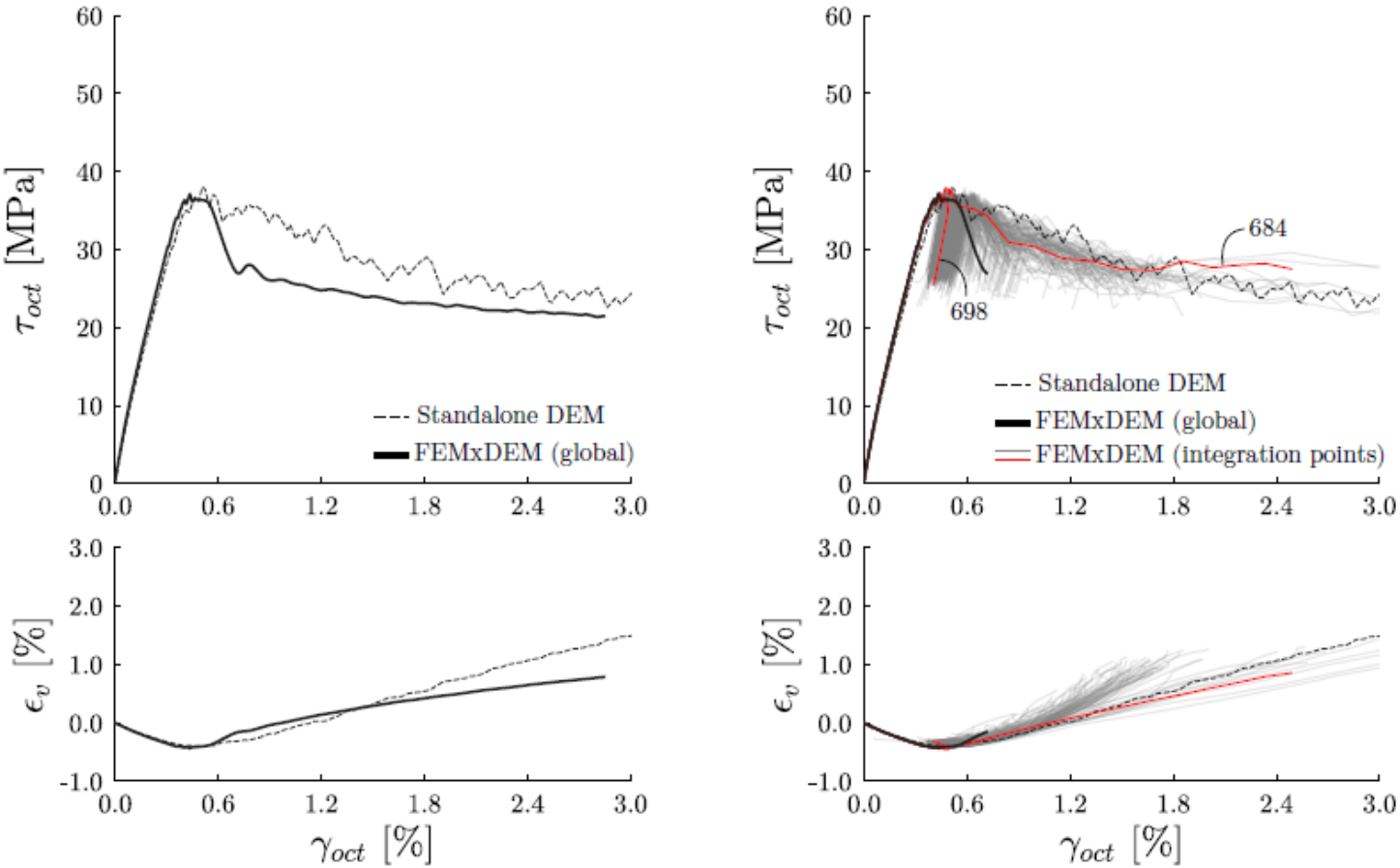

Incremental strain field

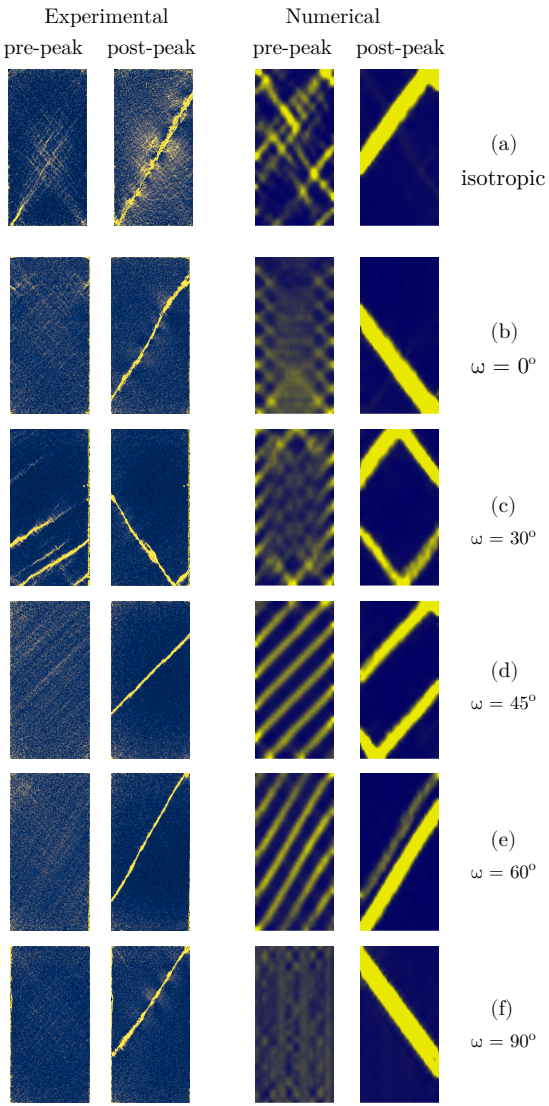

2. Bedding plane anisotropy 

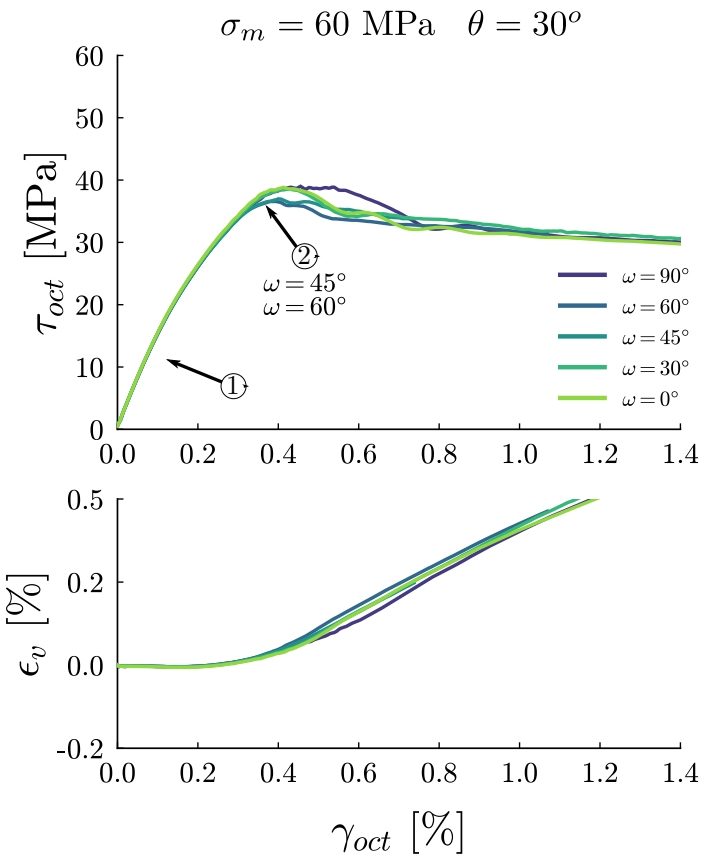

1. Initially similar mechanical response
2. Early divergence and transition into the softening regime

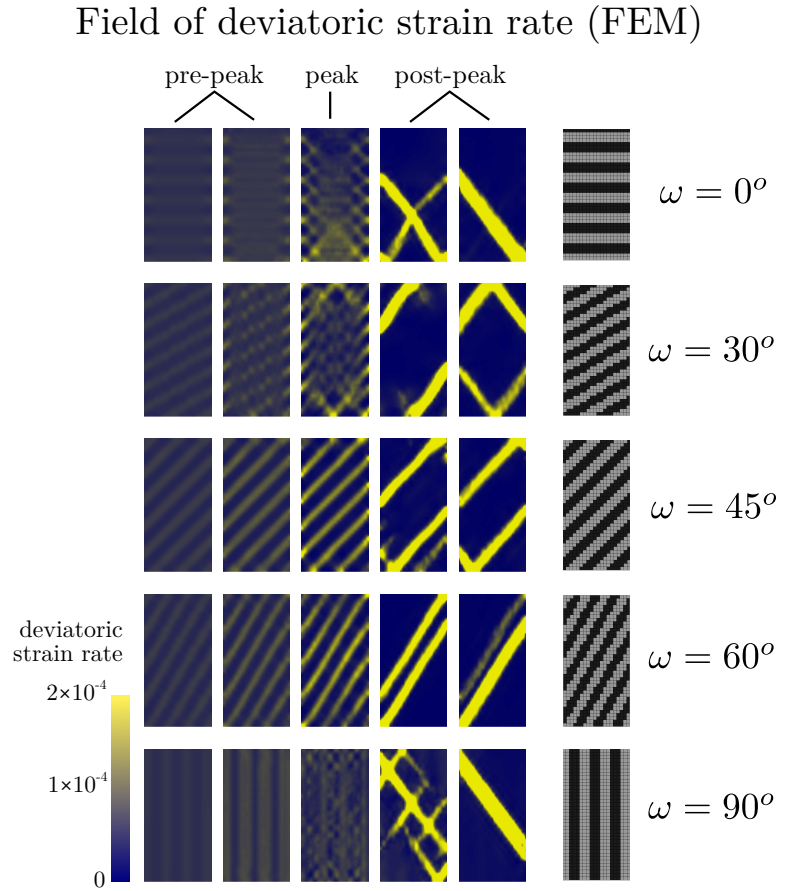

2. Concentration of strain inside the layer of loose EV
3. Influence of deformation band attractors